Used Fuel Disposition Campaign

Embrittlement and DBTT of High-Burnup PWR Fuel Cladding Alloys

Fuel Cycle Research & Development

Prepared for
U.S. Department of Energy
Used Fuel Disposition Campaign

M.C. Billone, T.A. Burtseva, Z. Han and Y.Y. Liu

Argonne National Laboratory
September 30, 2013
FCRD-UFD-2013-000401
ANL-13/16

Reviewed by:

Signature on file

Hanchung Tsai (Argonne National Laboratory)
Technical Reviewer

Submitted by:

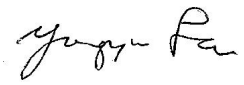

Yung Y. Liu (Argonne National Laboratory)
Work Package Manager

This page intentionally blank.

SUMMARY

Structural analyses of high-burnup (HBU) fuel require cladding mechanical properties and failure limits to assess fuel behavior during long-term dry-cask storage and transportation. Pre-storage drying-transfer operations and early stage storage subject cladding to higher temperatures and pressure-induced tensile hoop stresses relative to in-reactor operation and pool storage. Under these conditions, radial hydrides may precipitate during slow cooling and provide an additional embrittlement mechanism as the cladding temperature decreases below the ductile-to-brittle transition temperature (DBTT). On the basis of previous test results, susceptibility to radial-hydride precipitation depends on cladding material and microstructure, hydrogen content (C_H), and pre-drying hydride distribution, as well as peak hoop stresses and temperatures during drying operations and storage. Susceptibility to embrittlement depends on the extent of radial-hydride precipitation, the number density of circumferential hydrides, and the thickness of the outer-surface hydride rim. The goal of the testing program is to determine drying-storage conditions for which the cladding remains ductile at ambient temperature, in other words, with the DBTT ≤20°C.

Based on previous results, as-irradiated HBU M5® and ZIRLO™ exhibited high ductility at 20°C for a wide range of strain rates. Zircaloy-4 (Zry-4) with high C_H (640 wppm average and >840 wppm local C_H) was brittle at ≤90°C due to circumferential hydrides and was ductile at 20°C for lower C_H (<600 wppm C_H). Following simulated drying-storage at the Nuclear Regulatory Commission (NRC)-recommended limit (400°C), 140-MPa peak hoop stress prior to slow cooling (5°C/h) resulted in significant DBTT increases for HBU ZIRLO™ (185°C) and M5® (80°C) due to radial hydrides, while the DBTT for Zry-4 (620 wppm C_H) was only 55°C. Reducing the peak hoop stress to 110 MPa caused a reduction in DBTT to: 125°C for HBU ZIRLO™, 70°C for HBU M5®, and <20°C for HBU Zry-4 (520 wppm C_H). Metallographic results indicated that HBU M5®, with a recrystallized-annealed microstructure, was more susceptible to radial-hydride precipitation than HBU ZIRLO™, with a stress-relief-annealed microstructure. However, the opposite trend was observed for susceptibility to embrittlement due to the low C_H (<100 wppm) in HBU M5® relative to HBU ZIRLO™ (350 to 650 wppm) at comparable burnups. For HBU Zry-4 subjected to simulated drying and storage, embrittlement was primarily due to high concentrations of circumferential hydrides across about 50% of the cladding wall thickness.

Consistent with the goal of the testing program, the new work focused on the effects of lower peak cladding hoop stresses at 400°C to determine conditions for which the DBTT would be ≤20°C. HBU ZIRLO™ subjected to peak hoop stresses of 80 and 90 MPa exhibited DBTTs of <20°C and 20°C, respectively. Both sample materials contained about 530 wppm C_H. Along with the DBTT reduction, the effective lengths of radial hydrides decreased from 67% (for 140 MPa) to 30% (for 110 MPa) to 19% (for 90 MPa) to 9% (for 80 MPa) of the cladding wall thickness. A test was also conducted with HBU M5® with 90-MPa peak cladding hoop stress at 400°C. Following slow cooling, the DBTT was <20°C. The effective length of radial hydrides decreased with the decrease in peak hoop stress at 400°C: from 72% (for 140 MPa) to 61% (for 110 MPa) to 31% (for 90 MPa). However, because of the low C_H (about 60 to 90 wppm) in the HBU M5® samples, radial hydrides were thinner and spaced farther apart than the ones observed in HBU ZIRLO™ with much higher C_H. *In summary, a DBTT of ≤20°C can be achieved for peak drying-storage hoop stresses ≤110 MPa for HBU Zry-4 and ≤90 MPa for HBU ZIRLO™ and M5®.*

The drying process for casks containing HBU fuel assemblies may require multiple cycles to achieve ≤3-torr moisture content for 30 minutes while complying with the NRC-recommended peak cladding temperature limit (400°C). The HBU ZIRLO™ simulated drying-storage test for 90-MPa peak hoop stress at 400°C was repeated with two intermediate temperature cycles consisting of slow cooling from 400°C to 300°C and reheating to 400°C. The hold time between cycles was one hour. Literature results for non-irradiated, pre-hydrided Zry-4 show an increase in radial-hydride precipitation with temperature cycling at high stress (150 MPa). *However, no effects of multiple drying cycles were observed on radial-hydride lengths or DBTT with HBU ZIRLO™ subjected to 90-MPa peak hoop stress at 400°C.*

This page intentionally blank.

CONTENTS

FIGURES

TABLES

ACRONYMS, UNITS AND SYMBOLS

ACRONYMS

AMP = aging management plan

B&W TSG = Babcock and Wilcox Technical Service Group (formerly BWXT)

CoC = Certificate of Compliance

CWSRA = cold-worked, stress-relief annealed

DBTT = ductile-to-brittle transition temperature

H = hydrogen

HBU = high-burnup fuel

ISG = Interim Staff Guidance

LCO = limiting conditions of operation

LWR = light water reactor

NRC = Nuclear Regulatory Commission

ORNL = Oak Ridge National Laboratory

PWR = pressurized water reactor

RCT = ring compression test

RHCF = radial hydride continuity factor

RHT = radial-hydride treatment

RT =room temperature

RXA = recrystallized-annealed

TLAA = time-limited aging analysis

TMT = thermo-mechanical treatment

Zry-2 = Zircaloy-2

Zry-4 = Zircaloy-4

UNITS

°C = degree Celsius

GWd/MTU = giga-watt-days per metric tonne of uranium

h = hour

kN = kilo-Newton

m = meter

mm = millimeter

μm = micron

MPa = mega-Pascal

N = Newton

s = second

wppm = weight parts per million

SYMBOLS

C_H = hydrogen content in weight parts per million (wppm)

D_{mi} = inner diameter of cladding metal

D_{mo} = outer diameter of cladding metal

D_o = cladding outer diameter (includes outer-surface corrosion layer if present)

d_p = permanent displacement (pre-test diameter minus post-test diameter in loading direction)

d_p/D_{mo} = RCT permanent strain (%)

δ = controlled and measured RCT displacement at the 12 o'clock sample position

δ_{max} = maximum RCT displacement at the 12 o'clock sample position

ΔP = pressure difference across cladding wall ($P_i - P_o$)

δ_p = RCT offset displacement at 12 o'clock position relative to static support at 6 o'clock

δ_p/D_{mo} = RCT offset strain (%)

$(\varepsilon_\theta)_{max}$ = maximum hoop strain

h_m = cladding metal wall thickness

h_{ox} = thickness of outer surface corrosion (oxide) layer

K_{LM} = measured linearized loading slope (also known as loading stiffness)

K_{UM} = measured or calculated linearized unloading slope

L = length of RCT samples

L_R = length of continuous radial-circumferential hydrides projected onto cladding radius

M_{max} = maximum RCT bending moment

P = measured RCT load at the 12 o'clock sample orientation

P_i = internal gas pressure

P_{max} = maximum RCT load

P_o = external gas pressure

R_{mi} = inner radius of cladding metal

σ_θ = hoop stress

T = temperature

1. INTRODUCTION

Structural analyses of high-burnup (HBU) fuel rods require cladding mechanical properties and failure limits to assess fuel behavior during long-term dry-cask storage, post-storage retrieval and transportation, and post-transport retrieval. License applications for transport casks containing HBU fuel assemblies use properties and failure limits for as-irradiated cladding [1]. The Zircaloy-4 (Zry-4) properties and limits in Ref. 1 were based primarily on axial-tensile and pressurized-tube tests. Isotropic correlations were developed for stress vs. strain and failure limits. However, pre-storage drying-transfer operations and early stage storage subject cladding to higher temperatures and higher pressure-induced tensile hoop stresses relative to in-reactor operation and pool storage. Under these conditions, radial hydrides may precipitate during slow cooling and may introduce a potentially serious embrittlement mechanism as the cladding temperature decreases below the ductile-to-brittle transition temperature (DBTT).

In Interim Staff Guidance – 11, Revision 3 (ISG-11 Rev. 3), the Nuclear Regulatory Commission (NRC) recommends a peak cladding temperature limit of 400°C for drying-transfer operations, storage, and transport in casks containing HBU fuel [2]. Limits are also placed on the number of drying cycles and the temperature drop per cycle. One concern for HBU fuel cladding is the possible precipitation of radial hydrides, which could embrittle cladding in response to tensile hoop stresses caused by internal pressure loading and "pinch-type" loading during transport. Limits established in ISG-11 Rev. 3 relied on data available before 2002, which were primarily for low-burnup and non-irradiated/pre-hydrided Zry-4. At the time ISG-11 Rev. 3 was issued (2003), NRC recognized that data for HBU fuel cladding alloys were needed to determine the extent of radial-hydride embrittlement under conditions relevant to drying-transfer operations and storage. Data generated since 2002, mostly at Argonne, indicate that limits imposed by ISG-11 Rev. 3 do not prevent radial-hydride precipitation and radial-hydride-induced embrittlement in HBU cladding. Recent NRC reviews of applications for license renewal of the Prairie Island ISFSI and Amendment 5 of the Certificate of Compliance (CoC) for Transnuclear MP-197 have raised concerns with regard to the long-term storage and transportation of HBU fuel. The issues are summarized in "Compatibility of Requirements for Storage and Transportation of Spent Nuclear Fuel (Retrievability, Cladding Integrity, and Safe Handling)," a summary paper presented at the NRC Public Meeting to obtain stakeholder feedback on enhancements to the licensing and inspection programs for spent fuel storage and transportation under 10 CFR Parts 71 and 72 [3]. A major concern is whether or not HBU fuel will maintain cladding integrity and be readily retrievable after more than 20 years of storage. License approvals for the transport of HBU fuel assemblies have been delayed because of a lack of data for HBU fuel cladding after more than 20 years of storage, which corresponds to peak cladding temperatures of ≈200°C or less.

Argonne has developed a test protocol for studying HBU cladding embrittlement that has been used to generate data for NRC. Experimentally, the protocol involves two steps: (a) radial-hydride treatment (RHT), during which HBU cladding is exposed to simulated drying-storage temperature and hoop stress conditions, including slow cooling with decreasing stress, followed by (b) ring compression testing, in which rings sectioned from RHT HBU cladding are compressed to determine strength and ductility as a function of test temperature. The ring compression test (RCT) is used as a ductility screening test, and the RCT loading simulates pinch-type loading on HBU cladding that occurs during normal cask transport and drop accidents. The protocol was used to generate DBTT data for HBU ZIRLO™ and Zry-4 [4,5] (both NRC sponsored) and HBU M5® (DOE sponsored) [6]. Under DOE-sponsored research, Argonne has also generated baseline characterization data and data for the strength and ductility of as-irradiated Zry-4, ZIRLO™, and M5® that are important not only for determining the degrading effects of drying and early stage storage, but also for serving as reference properties for future evaluations of the effects of drying-storage on these cladding alloys [7–9].

The Argonne test protocol is described in detail in Ref. 4 and summarized in Refs. 5–9. For the convenience of the reader, it is summarized in Chapter 2 of this report.

In addition to the Argonne datasets for PWR cladding alloys, Aomi et al. [10] have generated data for Zry-2 and Zry-4 using test methods similar to the ones used by Argonne. However, RHT samples were cooled under constant stress (vs. decreasing stress, as used by Argonne), and RCTs were conducted only at room temperature (RT) and a slow displacement rate (0.033 mm/s vs. 5 mm/s used by Argonne). Their results are both revealing and relevant in evaluating the effects of hydrogen content (C_H) and thermo-mechanical treatment (TMT) on the susceptibility of cladding alloys to radial-hydride formation. Test results indicate that susceptibility to radial-hydride precipitation during cooling is dependent on cladding alloy, TMT, total C_H, C_H below the hydride rim, and peak RHT temperature and hoop stress. The combination of recrystallized-annealed (RXA) microstructure and low C_H (above the inner liner for Zry-2) makes Zry-2 and M5® highly susceptible to precipitation of long radial hydrides during cooling. For cold-worked, stress-relief annealed (CWSRA) alloys, ZIRLO™ was found to be more susceptible to radial-hydride precipitation than Zry-4. It has been speculated that differences in distribution of hydrides across the cladding wall (lower for ZIRLO™ below the hydride rim) may be responsible for this behavior [5].

Previous Argonne data for as-irradiated, HBU cladding and HBU cladding subjected to simulated drying-storage conditions (RHT) are summarized in Chapter 3. For HBU cladding subjected to peak RHT conditions of 140-MPa and 110-MPa cladding hoop stresses at 400°C followed by slow cooling (5°C/h) under decreasing hoop stress, DBTT values were determined as a function of peak RHT hoop stress: (a) for 140-MPa peak hoop stress, 185°C for ZIRLO™, 80°C for M5®, and 55°C for Zry-4 and (b) for 110-MPa peak hoop stress, 125°C for ZIRLO™, 70°C for M5®, and <20°C for Zry-4. With the exception of Zry-4, the DBTTs determined in the previous work were above target values (≤20°C) for peak RHT hoop stresses ≥110 MPa

In the completed FY2013 work described in this report, the peak RHT hoop stresses for HBU ZIRLO™ and M5® were systematically lowered until their DBTTs were ≤20°C. In addition, the effects of multiple dying cycles on DBTT were investigated with a HBU ZIRLO™ sample.

2. HBU CLADDING MATERIALS AND TEST METHODS

2.1 HBU Cladding Materials

Table 1 summarizes characteristics of the HBU cladding segments, each about 80 mm long, used for baseline studies of as-irradiated cladding and for studies of cladding ductility following simulated drying-storage (RHT). The material came from fuel rods irradiated to HBU in commercial LWRs. The M5® cladding segment listed at 63 GWD/MTU was irradiated in one of the Ringhals reactors and defueled by Studsvik, both in Sweden. M5® cladding segments listed at 68 and 72 GWd/MTU came from fuel rods irradiated in the same assembly in the North Anna reactors. These segments were defueled by BWXT (now B&W TSG). ZIRLO™ cladding segments came from two fuel rods irradiated in the same assembly in the North Anna Reactors. These segments were defueled by Studsvik. Zry-4 cladding segments came from two fuel rods irradiated in the same assembly in one of the H.B. Robinson reactors. These segments were defueled by ORNL. As discussed in Chapter 3, the ± C_H values represent one-sigma variations in data collected from multiple axial locations along each segment and quarter-ring samples at each axial location. In general, the large one-sigma values were due to circumferential variation in C_H, especially for average C_H values ≥350 wppm. Additional characterization results are presented in subsequent chapters: outer diameter of corroded cladding (D_o), corrosion-layer (i.e., outer-surface oxide-layer) thickness (h_{ox}), cladding metal outer diameter (D_{mo}), and cladding metal wall thickness (h_m).

Table 1. Summary of cladding materials used for baseline studies of as-irradiated cladding and studies of cladding ductility following simulated drying-storage (RHT) at 400°C peak RHT temperature.

Cladding Alloy	TMT	Burnup, GWd/MTU	Hydrogen Content, wppm	Peak RHT Stress, MPa	Number of Drying Cycles	References
M5®	RXA	72	76±5	–	–	7–9
		63	94±4	140	1	6
		68	72±10	110	1	6
		68	58±15	90	1	This report
ZIRLO™	CWSRA	68	530±70	–	–	7–9
		70	650±190	140	1	4–5
		70	425±63	110	1	4–5
		70	350±80	110	1	4–5
		68	530±100	90	1	This report
		68	480±131	90	3	This report
		68	535±50	80	1	This report
Zry-4	CWSRA	67	640±140	–	–	7–9
		67	300±15	–	–	This report
		67	615±82	140	1	4–5
		67	520±90	110	1	4–5

2.2 Test Protocol

The test protocol consisted of two steps: (a) simulated drying and storage (called RHT) during which a sealed, pressurized rodlet is heated to 400°C, held at 400°C for one hour, cooled slowly at 5°C/h to 200°C

(135°C for low-C_H M5®), and cooled at a faster rate to room temperature (RT) and (b) ring-compression testing at three to four temperatures from RT to 200°C and at 5 mm/s (reference value) displacement rate to a maximum displacement of 1.7 mm.

HBU cladding segments were used to fabricate sealed and pressurized (with argon) rodlets. Bottom and top end fixtures fabricated from Zircadyne-702 were welded circumferentially to each cladding segment using an Astro Arc welder in a controlled argon environment. The cladding-segment/end-fixture remained stationary, and the weld head rotated around the joint to be welded. A zirconia pellet (25-mm-long) was inserted into the rodlet to reduce the stored energy. The heat-affected zone was relatively narrow for the weld head design and the welding parameters used. The top end fixture contained a small hole to allow for pressurization of the rodlet. RT pressures were selected to achieve target values of pressure and cladding hoop stress at 400°C. Following circumferential welding and pressurization in a specially designed sealed chamber with a sapphire lens for the laser beam, the small hole was sealed by laser welding. Leak testing was performed within the pressurization chamber. The corrosion and fuel-cladding bond layers were removed by mechanical means from about 15 mm of each segment end to ensure a high-quality metal-to-metal weld of the end fixtures. During this process, some of the cladding metal was also removed between these layers. Figure 1 shows a non-irradiated 17×17 cladding segment before (upper photo) and after (lower photo) fabrication of the pressurized rodlet.

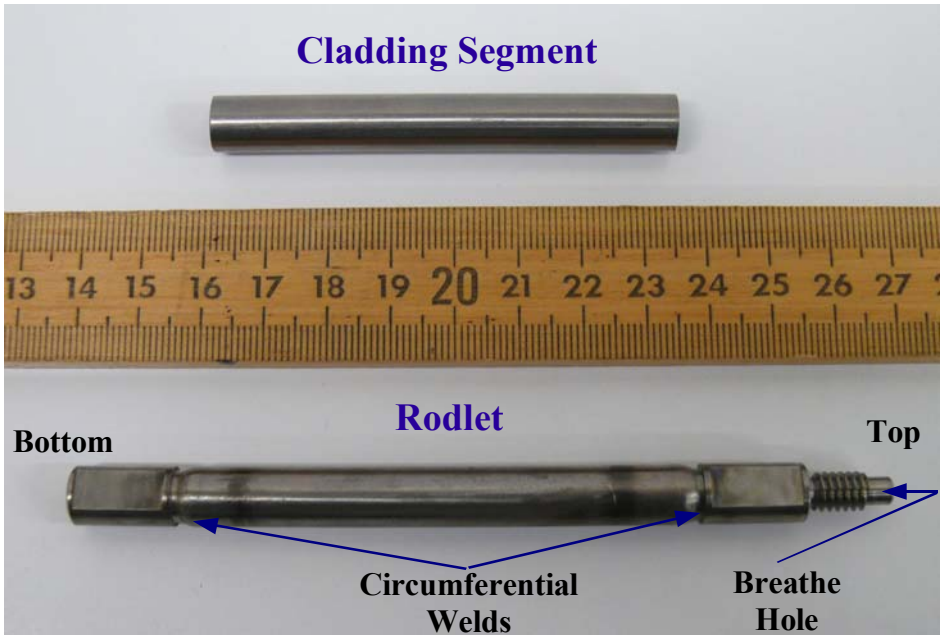

Figure 1. Cladding segment prior to rodlet fabrication (top image) and after rodlet fabrication.

Prior to rodlet pressurization, the outer diameter was measured for each corroded segment at two orientations (90° apart) and at three axial locations. These values were averaged to give D_o. The value of h_{ox} was estimated from sibling rod data or from interpolation-extrapolation of data from the same rod at different axial locations. The same approach was used to estimate h_m. The value of D_{mo} was calculated from $D_o - 2\ h_{ox}$, and the metal inner diameter (D_{mi}) was calculated from $D_{mo} - 2\ h_m$. The ratio R_{mi}/h_m, where R_{mi} is the metal inner radius, was used in Eq. 1 to calculate the average hoop stress (σ_θ) from the

pressure difference ($\Delta P = P_i - P_o$) across the cladding wall, where P_o was 0.1 MPa during RT (23°C) fabrication and 0.17 MPa in the RHT furnace. The ideal gas law was used to relate the absolute pressure at 400°C to the RT pressure according to P_i (400°C) = (673K/296K) P_i (23°C). Given the target σ_θ value at 400°C, the RT pressure can be determined from Eq. 1 and the information given above.

$$\sigma_\theta = (R_{mi}/h_m)\,\Delta P \qquad (1)$$

Following RHT (see Fig. 2 for part of the reference temperature history), the rodlet was depressurized and sectioned for C_H samples, RCT samples, and metallographic imaging samples, which allowed precise determination of the geometrical factors in Eq. 1. Using this procedure, the calculated peak rodlet stress was within 2 MPa of the target value.

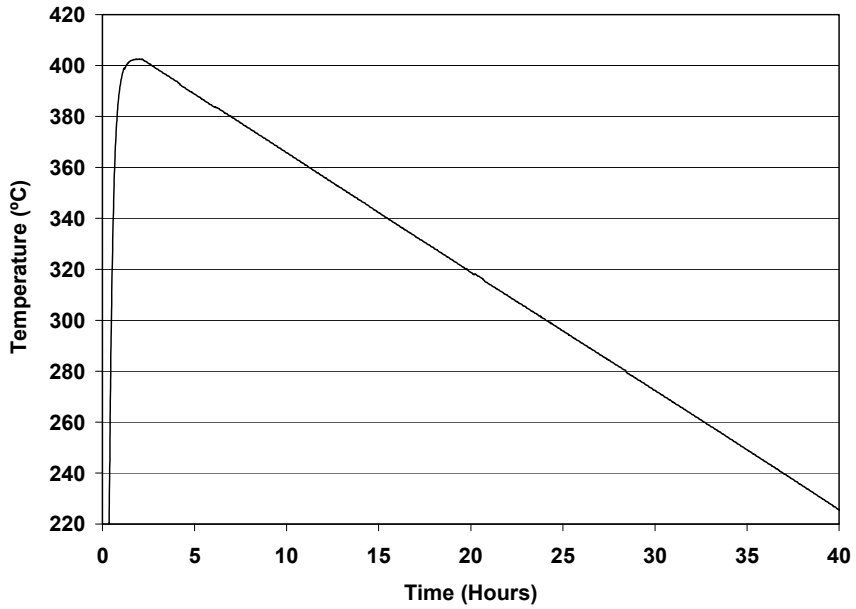

Figure 2. Reference cladding temperature history for one-cycle RHT with a hold time of one hour at 400°C.

The second phase of the test protocol consisted of RCTs. Figure 2 shows a schematic of RCT loading. The RCT load induces maximum hoop bending stresses (σ_θ) at the inner surfaces of the 12 (under load) and 6 (above support) o'clock positions. Tensile hoop stresses also occur at the 3 and 9 o'clock outer surfaces. Associated with these maximum tensile stresses are maximum tensile strains (ε_θ). Within the elastic range, these hoop stresses at 3 and 9 o'clock are ≈60% of the maximum stresses at 12 and 6 o'clock. Also, because the length (L ≈ 8 mm) of the rings is much greater than the cladding wall thickness (h_m = 0.54 to 0.75 mm), an axial stress is induced that is 0.37 times the hoop stress within the elastic deformation regime. The maximum displacement (1.7 mm) was chosen to give ≈10% offset strain at RT. The reference displacement rate was 5 mm/s.

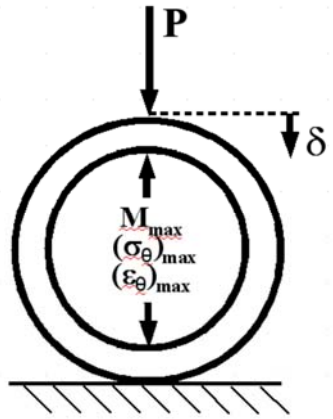

Figure 3. RCT loading (P). Tests are conducted in the displacement (δ)-controlled mode to 1.7-mm maximum displacement. M_{max} is the maximum bending moment.

Load-displacement curves and post-test examination were used to determine offset displacements (δ_p) and permanent displacements (d_p), respectively. These were normalized to D_{mo} to give relative plastic displacement (i.e., plastic strain) for the ring structure. Permanent displacement is defined as the difference between pre- and post-test diameter measurements along the loading direction. Figure 4 shows how traditional and corrected offset displacements were determined from a benchmark load-displacement curve for a non-irradiated M5® ring. The traditional offset methodology calls for unloading the sample at the same slope as the measured loading slope (i.e., stiffness). It should be noted that this slope is less than the calculated sample stiffness due to the influence of machine compliance. This approach gave a traditional δ_p = 1.19 mm. However, there is an inherent error in this approach as the measured unloading slope (≈0.83 kN/mm) is always less than the loading slope for δ_p/D_{mo} >2%. The decrease in unloading-stiffness/loading-stiffness increases with δ_p/D_{mo} and is 24% for the 12.6% δ_p/D_{mo} shown in Fig. 4. Using the measured unloading stiffness, the corrected δ_p is 1.19 mm, which is close to the measured d_p (1.05 mm). On the basis of error analyses and data trends, rings with d_p/D_{mo} <1% or δ_p/D_{mo} <2% are classified as brittle.

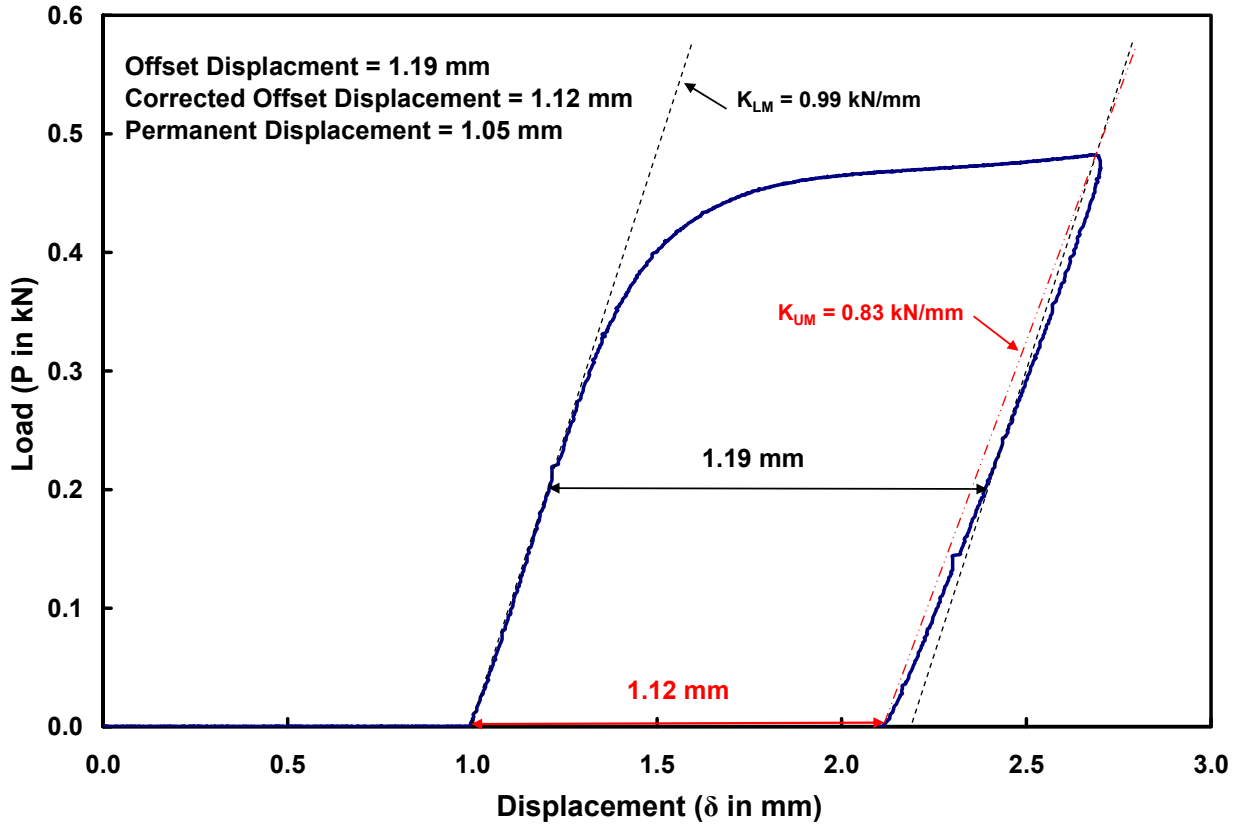

Figure 4. Load-displacement curve for non-irradiated M5® ring tested at RT and 5 mm/s to 1.7-mm displacement. Sample dimensions were 7.7-mm L, 9.48-mm D_{mo}, and 0.63-mm h_m.

For rings that crack during the 1.7-mm displacement, d_p cannot be determined accurately. Thus, one must rely on the corrected offset displacement prior to the first significant crack to determine ductility. The embrittlement criterion established for cladding with radial hydrides was δ_p/D_{mo} <2% prior to >25% load drop, which corresponded to a crack through >50% of the wall [4,5]. One of the purposes of the baseline studies was to examine the relationship between load drop and extent of wall cracking for as-irradiated cladding with primarily circumferential hydrides.

In order to determine the corrected offset displacement and strain for rings that crack prior to 1.7-mm displacement, a linear relationship was derived between the ratio of unloading stiffness (K_{UM}) and loading stiffness (K_{LM}) and the traditional offset strain for $\delta_p/ D_{mo} \geq 2\%$

$$K_{UL}/K_{UM} = 1 - 0.025\ (\delta_p/ D_{mo} - 2\%) \qquad (2)$$

This page intentionally blank.

3. SUMMARY OF PREVIOUS DATA BASE

3.1 Baseline Studies for As-Irradiated Cladding

Detailed characterization was performed for as-irradiated HBU cladding segments. For cladding materials with a hydride rim (i.e., ZIRLO™ and Zry-4), additional results were obtained for the C_H within the inner two-thirds of the cladding wall. In Refs. 4-5, it was speculated that cladding materials with <200 wppm C_H (i.e., solubility limit at 400°C) within this region might be more susceptible to radial-hydride precipitation than materials with >200 wppm C_H. Table 2 summarizes characterization results.

Table 2. Characterization results for HBU cladding segments used in baseline studies.

Parameter	17×17 M5®	17×17 ZIRLO™	15×15 Zry-4	
Burnup, GWd/MTU	72	68	67	**67**
ANL Segment ID	652E6	105A	606C2	**605D3**
D_o, mm	9.53	9.53	10.75	**10.75**
h_{ox}, μm	8±1	47±11	95±5	**39±5**
D_{mo}, mm	9.51	9.44	10.56	**10.67**
h_m, mm	0.55	0.54	0.69	**0.75**
C_H (Corroded Cladding), wppm	76±5	530±70	640±140	**300±25**
C_H (Inner 66% of Wall), wppm	≈76	136±7	246±29	**160±7**

Metallographic images for the cladding cross section are shown in Section 3.2 to serve as references for images of cladding cross sections following RHT.

RCTs were conducted with as-irradiated HBU PWR cladding samples at three RT displacement rates and two to three temperatures to determine strain-rate and temperature sensitivity for strength (maximum RCT load, P_{max}) and ductility (corrected offset strain and permanent strain).

Table 3 summarizes RCT results for as-irradiated HBU M5®. Rings were 7.6–8.0 mm long. The strength (maximum load P_{max}) was normalized to 8.0 mm to allow direct comparison of results. As none of the samples cracked, offset and permanent strains represent maximum values attained after 1.7-mm δ. The ductility at RT showed no displacement-rate sensitivity for the 1000-fold increase (from 0.05 to 50 mm/s). The strength increase was relatively small (11%) for the large increase in displacement rate. The strength decrease (9%) with temperature elevation was also modest. Thus, HBU M5® exhibited high ductility with relatively low sensitivity to displacement rate and temperature within the conditions tested.

Table 4 summarizes RCT results for as-irradiated HBU ZIRLO™. Rings were 7.1–8.1 mm long. The RCT at low displacement rate (0.05 mm/s) and RT caused a 39% load drop at ≈7% offset strain. The test was rerun with ring 105A8 and terminated after a 37% load drop at ≈8% offset strain. Two major cracks were observed at the 3 and 9 o'clock orientations, which extended from the outer surface into ≈50% of the wall. Very little change in strength or ductility was observed with the 1000-fold increase in displacement rate: (a) ≈8% increase in strength and (b) ductility decrease from 7.8±0.1.0% to 5.5%. For the ring tested at 150°C, there was an increase in ductility and a small (11%) decrease in strength. Cracking occurred near the end of the 90°C RCT: one 60% wall crack and 13 minor cracks were observed. Five minor cracks were observed in the 150°C RCT sample. Thus, the ductility of as-irradiated HBU ZIRLO™ exhibited mild temperature sensitivity, but all results were above the DBTT.

Table 3. Summary of RCT results for as-irradiated HBU M5® cladding samples. P_{max} was normalized to a sample length of 8.0 mm.

Sample ID	Length, mm	Displacement Rate, mm/s	RCT T, °C	Normalized Pmax, N	Offset Strain, %	Permanent Strain, %
652E6D	7.86	0.05	26	525	9.8	9.1
652E6E	8.02	5	26	553	9.8	9.6
652E6K	7.72	50	26	581	8.7	8.8
652E6C	7.66	5	60	528	9.7	9.5
652E6L	7.62	5	90	506	10.0	9.9

Table 4. Summary of RCT results for as-irradiated HBU ZIRLO™ cladding samples. P_{max} was normalized to a sample length of 8.0 mm to allow comparison with the M5® results in Table 3.

Sample ID	Length, mm	Displacement Rate, mm/s	RCT T, °C	Normalized P_{max}, N	Offset Strain, %	Permanent Strain, %
105A7	7.90	0.05	20	560	6.7	---
105A8	7.06	0.05	20	529	8.8	---
105A9	7.80	5	20	584	7.0	---
105A10	7.61	50	20	591	5.5	---
105A12	7.52	5	90	553	10.4	---
105A11	8.08	5	150	525	10.9	10.2

Table 5 summarizes RCT results for as-irradiated HBU Zry-4. For high-C_H rings from segment 606C2, the average offset strain was <2% prior to an average load drop of ≈30%. Sensitivity of ductility to displacement rate and temperature could not be assessed from these data. Based on maximum loads prior to ≈30% load drops, strength showed very little sensitivity to displacement rate and temperature (5% decrease at 90°C). The second low-rate RCT was terminated after a 27% load drop. A single crack developed at 9 o'clock, which extended from the outer surface into ≈40% of the wall. Two 70% wall cracks developed at 3 and 9 o'clock for the RT test at 5 mm/s to 1.7 mm δ_{max}. To verify that the high density of circumferential hydrides caused the embrittlement of the 606C2 samples, an RCT was conducted at RT and 5 mm/s for the lower-C_H (300 wppm) ring 605D3F2. The material exhibited high ductility with no cracking through 1.7 mm δ_{max}. Thus, the HBU Zry-4 metal matrix does indeed have high ductility in response to RCT loading. Load-displacement curves for low- and high-C_H Zry-4 are compared in Fig. 5.

Table 5. RCT results for as-irradiated HBU Zry-4 cladding samples. P_{max} was normalized to 8.0-mm sample length. Sample 605D3F2 had low C_H (300±15 wppm).

Sample ID	Length, mm	Displacement Rate, mm/s	RCT Temp., °C	Normalized P_{max}, N	Offset Strain, %	Permanent Strain, %
606C2G	7.76	0.05	23	989	1.3	---
606C2H	7.81	0.05	20	924	2.3	---
606C2J	7.58	5	23	1010	1.5	---
606C2K	7.97	50	25	996	1.5	---
606C2L	7.69	5	90	958	1.5	---
605D3F2	8.02	5	22	1111	>9.9	>7.6

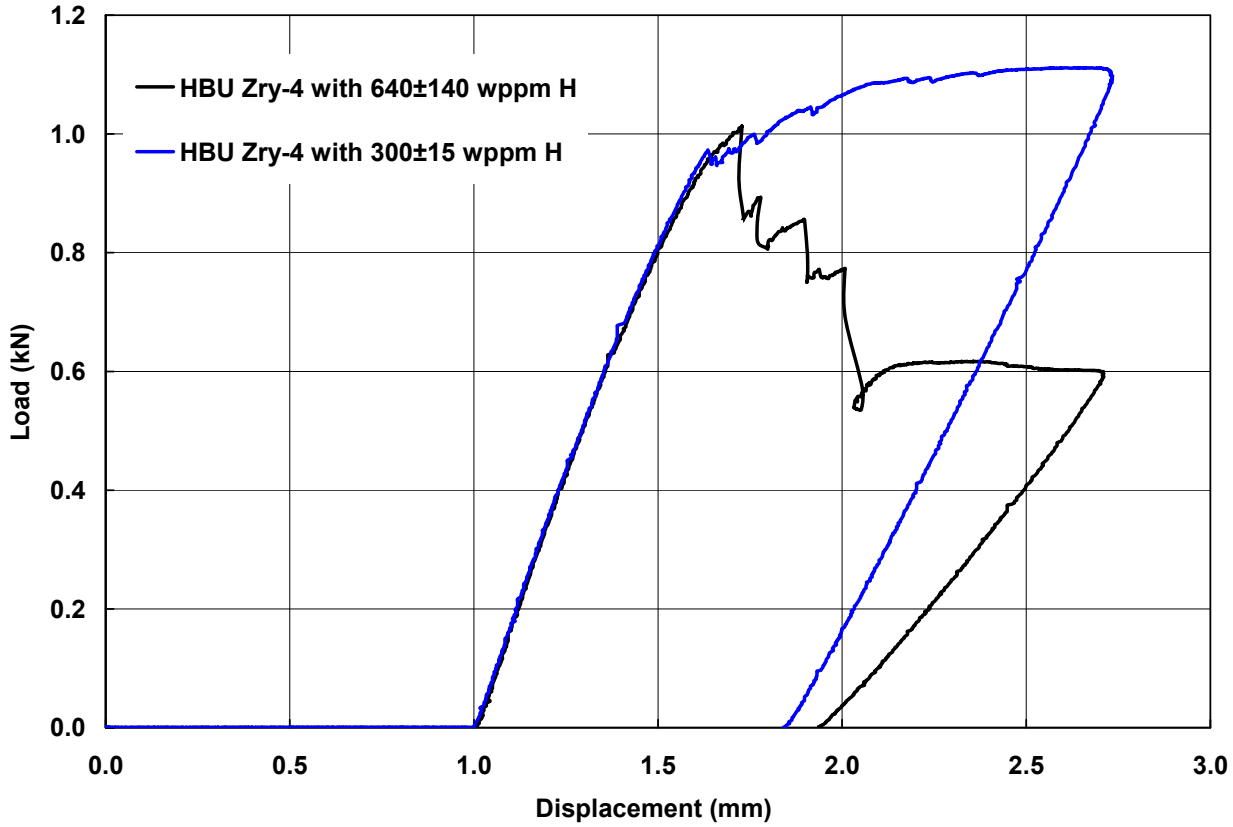

Figure 5. Load-displacement curves for HBU Zry-4 with high (640±140 wppm) and low (300±15 wppm) C_H. RCT tests conducted at RT and 5 mm/s displacement rate.

Metallographic imaging was used to confirm that the ring with 640±140 wppm C_H cracked in the high C_H region while the ring with 300±15 wppm experienced no cracking. Figure 6 shows the 3 o'clock orientation for both rings. At this orientation, the 70% wall crack can be observed for the high-C_H ring (Fig. 6a). Cracking initiated at the cladding outer surface where the maximum tensile bending stress occurred for that location. As shown in Fig. 6b, the low-C_H ring experienced no cracking in the cladding metal. As predicted, finely spaced radial cracks were observed in the corrosion layer. However, these did not extend into the hydride rim within the metal cladding.

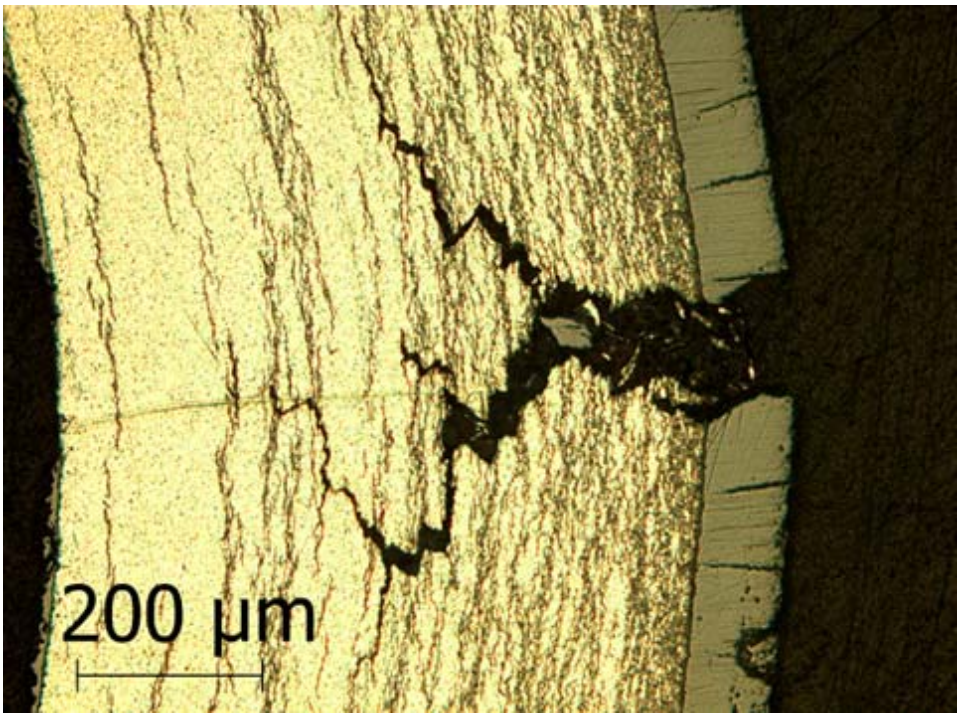

(a)

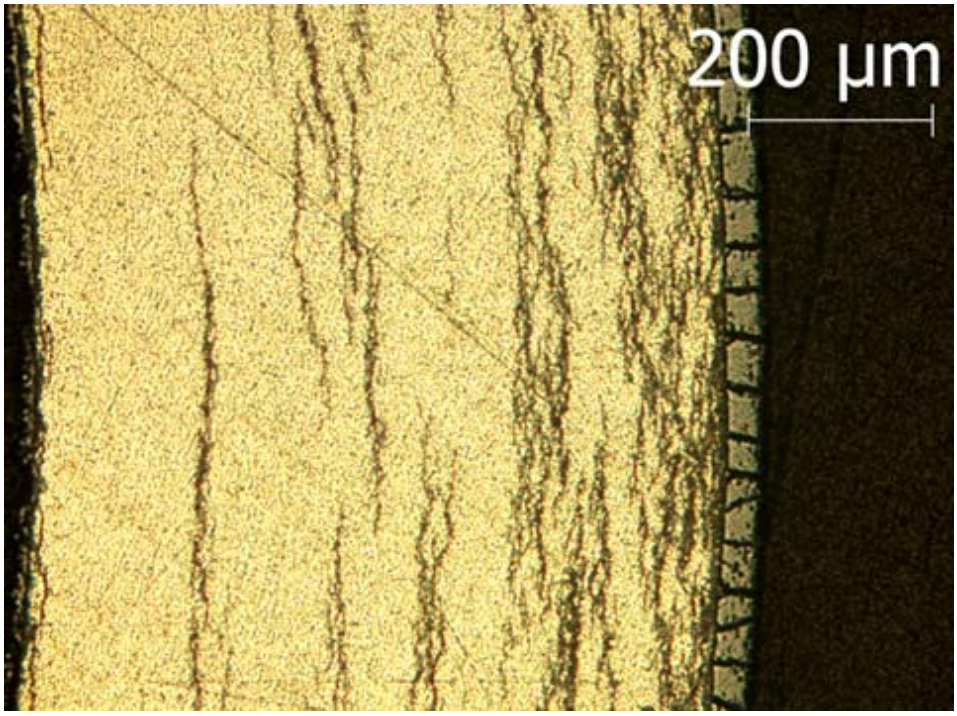

(b)

Figure 6. Post-RCT images of as-irradiated HBU Zry-4 at the 3 o'clock orientation: (a) high-C_H (640±140 wppm) ring and (b) low-C_H (300±15 wppm) ring.

3.2 Summary of Previous Results for HBU Cladding after RHT

3.2.1 HBU M5® after RHT

Load-displacement curves are given in Ref. 6 for HBU M5® following RHT at peak 400°C hoop stresses of 140 MPa and 110 MPa and slow cooling from 400°C at 5°C/h. Figure 7 shows offset strain vs. RCT test temperature for these two sets of RHT conditions, as well as the baseline results for as-irradiated M5®. For both RHT stress conditions, RCT samples were classified as brittle (<2% offset strain) at RT and 60°C and ductile at T ≥90°C. The DBTT was estimated to be 80°C for the 140-MPa RHT and 70°C for the 110-MPa RHT.

Figure 8 compares the 60°C load-displacement curve for the 140-MPa RHT sample to the baseline results at 26°C for HBU M5®. The 140-MPa RHT sample loads (7.50-mm length) were normalized to 8.0 mm (baseline sample length). The first load drop for the RHT ring occurred during elastic loading at P = 267 N. After the load drop, loading increased at a linear rate to 324 N. On the basis of a >50% decrease in stiffness (i.e., loading slope), it was concluded that a crack had grown through >50% of the wall at the first load drop initiating from 267 N. Thus, P_{max} = 267 N and δ_p/D_{mo} = 0% for the RHT sample. By contrast, RT results for as-irradiated M5® were P_{max} = 553 N and δ_p/D_{mo} > 10%. Thus, the degradation in RCT properties due to RHT can be quantified as a 52% decrease in P_{max} and a ductility decrease from >10% to 0% for RCT temperatures below the DBTT.

Figure 9 shows the hydride distribution and orientation in HBU M5® in the as-irradiated condition (Fig. 9a), after RHT at 400°C and 140-MPa peak hoop stress (Fig. 9b), and after RHT at 400°C and 110-MPa peak hoop stress (Fig. 9c). For M5® following RHT, primarily long radial hydrides precipitated during the 5°C/h cooling from 400°C. The longest radial hydride observed in Fig. 9b had a length that is 80% of the wall thickness. These radial hydrides provided pathways for crack initiation and propagation in response to hoop-stress loading. For both the 140-MPa and 110-MPa RHT rodlets, 36 images (3 axial locations and 12 orientations per location) were taken. The longest radial hydride in each image was normalized to the cladding wall thickness and averaged to obtain the radial-hydride continuity factor (RHCF): 72±10% for 140-MPa RHT and 61±10% for 110-MPa RHT. For the post-RHT RCT at 60°C, Fig. 8 shows three load drops. Although each load drop may represent simultaneous crack initiation and propagation through part of the wall, a simplistic interpretation would be that the first load drop in the elastic regime represents initiation of a single crack extending through >50% of the wall thickness, the second load drop represents the same for a second crack, and the third load drop—which is large—represents initiation and propagation of two additional cracks. Following RCT, major cracks were observed at four locations: 12 o'clock (see Fig 10a), 3 o'clock, 6 o'clock (see Fig. 10b), and 9 o'clock. Metallographic examination was performed for a cross section at the sample mid-span. The 12 o'clock crack was partial-wall, but it extended through >50% of the wall. The other three cracks were essentially through-wall cracks, like the one imaged in Fig. 10b.

Strength and ductility results from RCTs for as-irradiated HBU M5® and HBU M5® following RHT are summarized in Table 6.

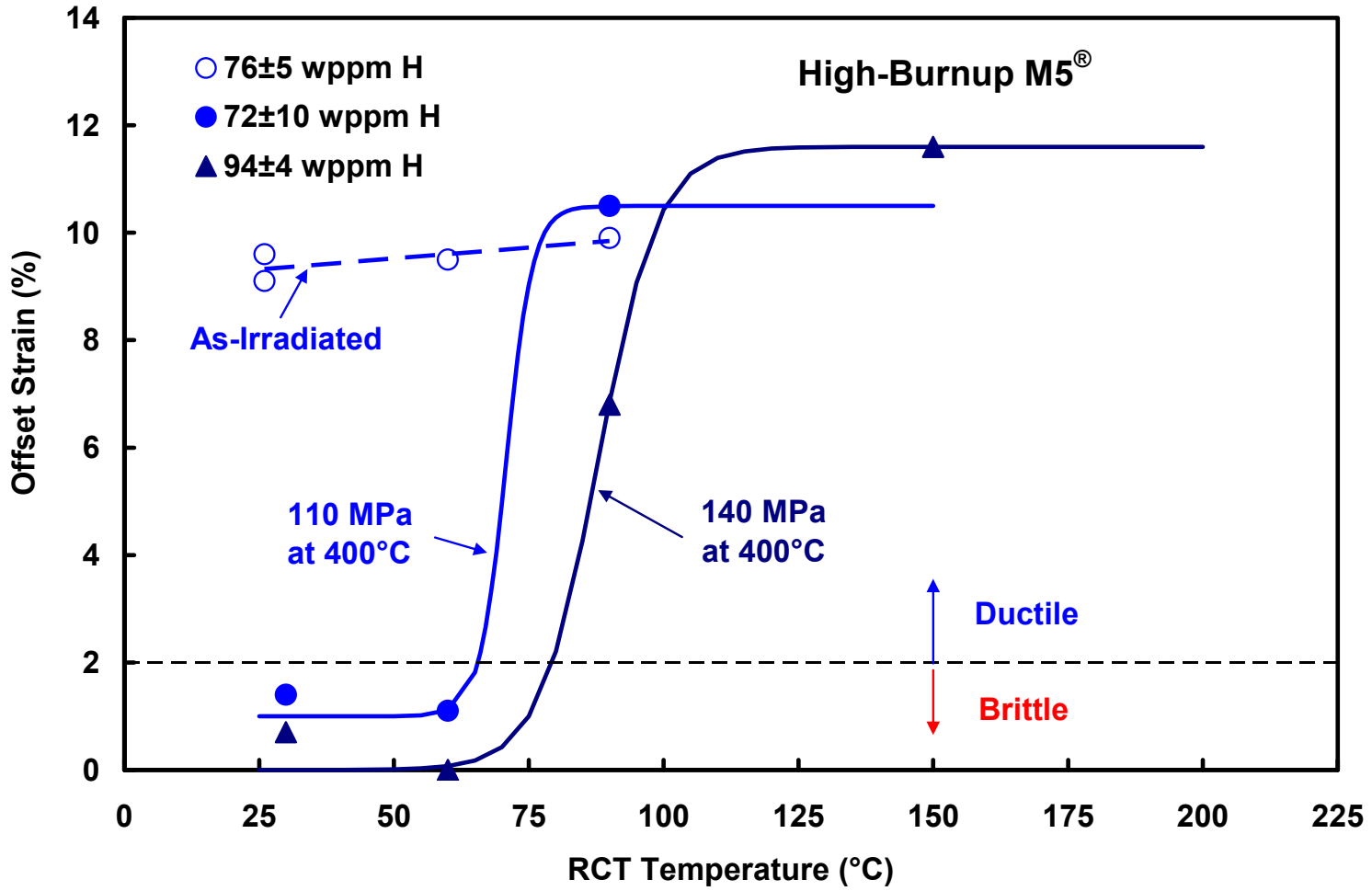

Figure 7. RCT offset strains vs. RCT temperature for HBU M5® following irradiation and following RHT at peak 400°C hoop stresses of 140 MPa and 110 MPa.

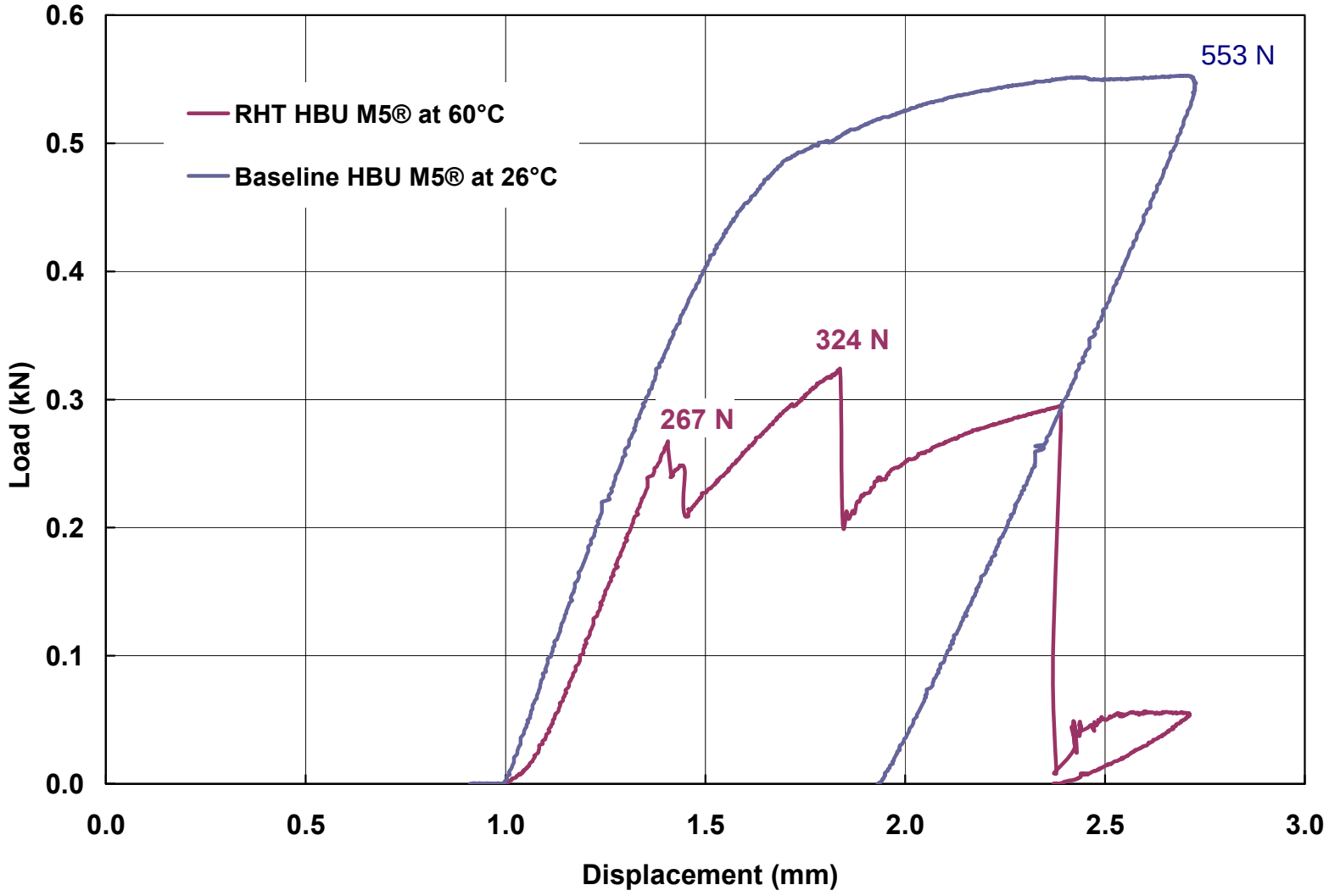

Figure 8. RCT load-displacement curves for HBU M5®: (a) as-irradiated (i.e., baseline) condition (see Fig. 9a) prior to drying-storage and tested at 26°C and (b) following RHT at 400°C and 140 MPa (see Fig. 9b) and tested at 60°C.

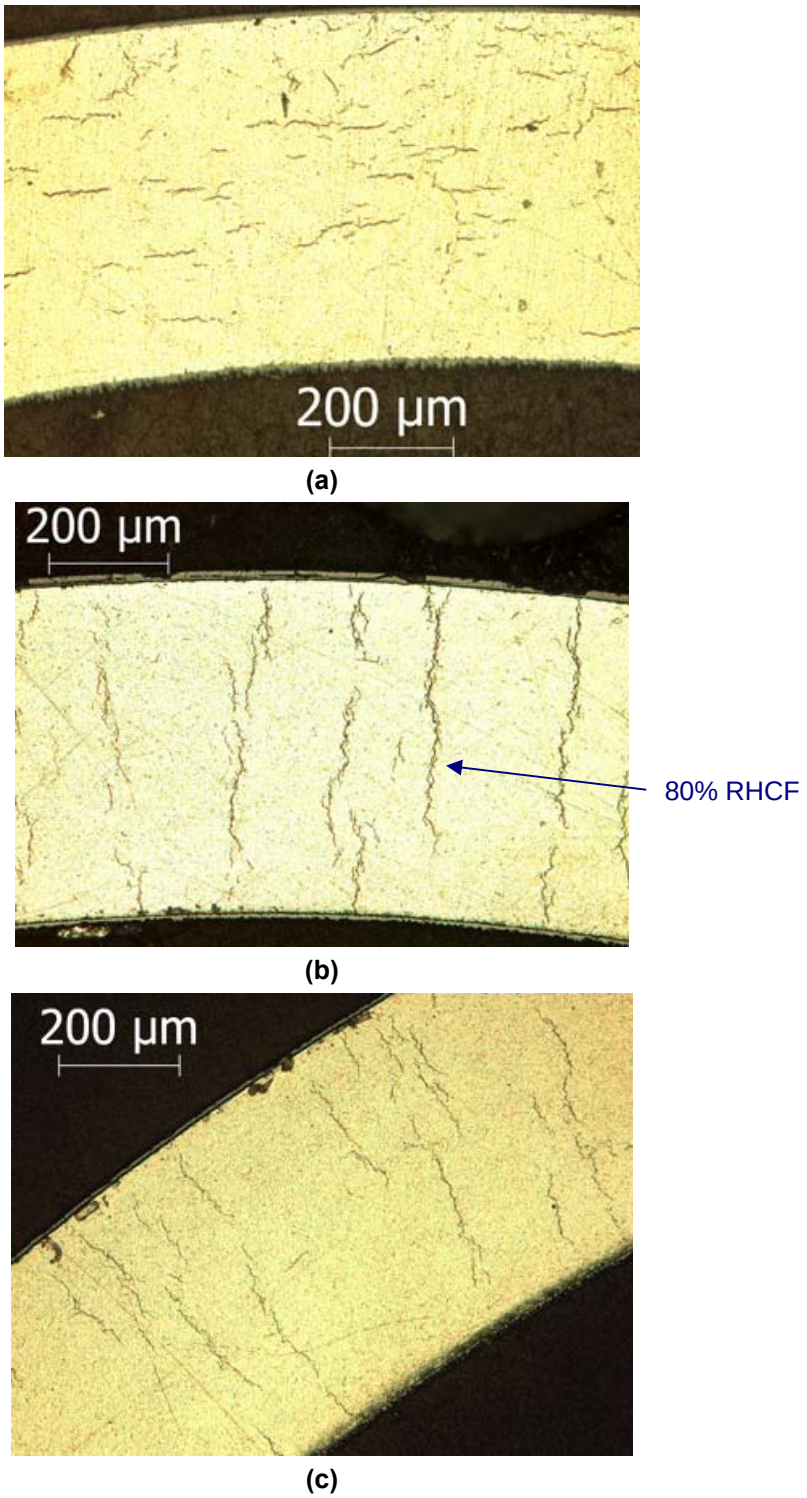

Figure 9. Hydride distribution and orientation in HBU M5®: (a) as-irradiated (baseline) with 76 wppm C_H, (b) after RHT at 400°C and 140 MPa with 94 wppm C_H, and (c) after RHT at 400°C and 110 MPa with 72 wppm C_H.

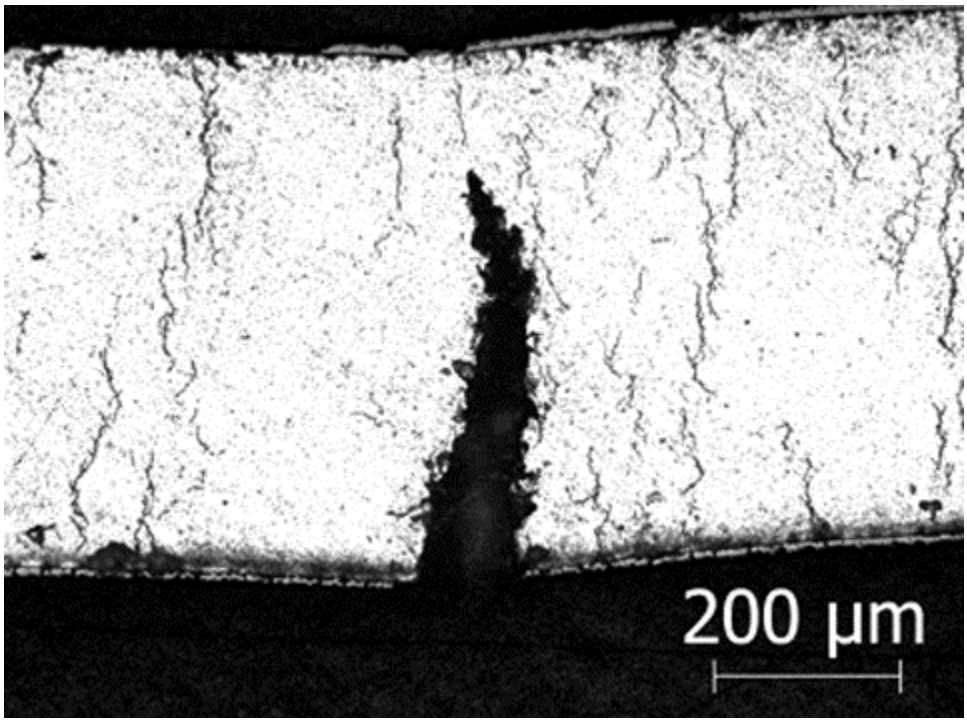

(a)

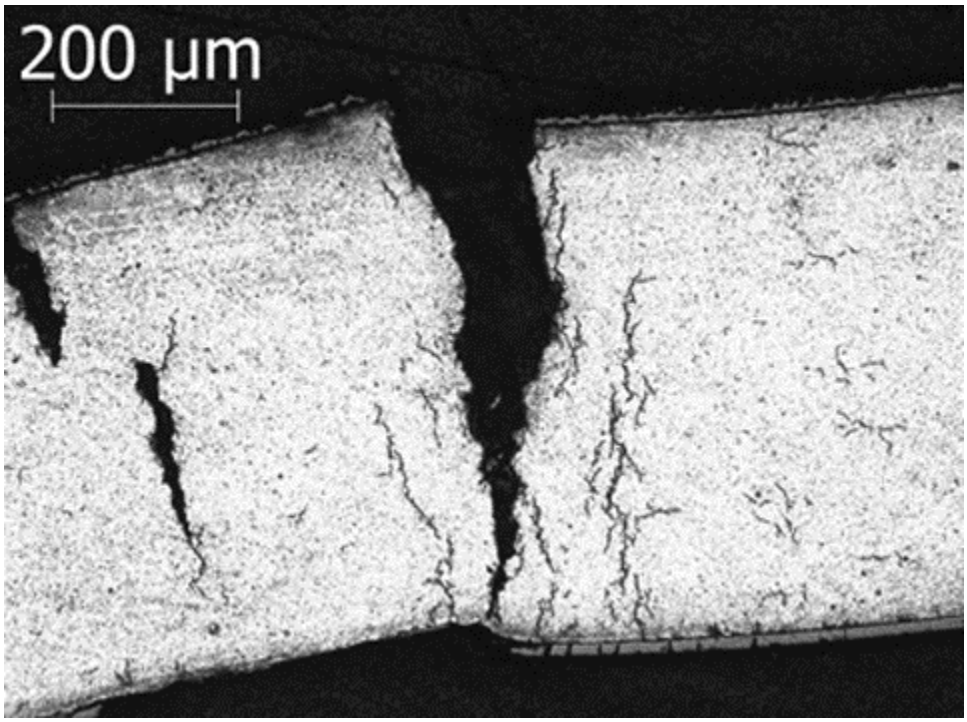

(b)

Figure 10. Two of four major cracks observed in the post-RCT metallographic images for RHT (400°C and 140 MPa) HBU M5® tested at 60°C: (a) 12 o'clock location and (b) 6 o'clock location.

Table 6. Summary of strength (P_{max}) and ductility (δ_p/D_{mo}) results for HBU M5® in the as-irradiated condition (i.e., baseline results for 652E6E) and following RHT. P_{max} was normalized to 8-mm sample length to determine the percentage decrease in maximum load relative to the baseline result.

Sample ID	Peak RHT T, °C	Peak RHT σ_θ, MPa	RCT T, °C	Reduction in P_{max}, %	Ductility δ_p/D_{mo}, %
652E6E	---	---	26	0	>10
645D8	400	140	30	34	0.7
645D3	400	140	60	52	0
645D10	400	140	90	20	6.8
645D5	400	140	150	21	>12
651E5H	400	110	30	22	1.4
651E5C	400	110	60	28	1.1
651E5F	400	110	90	17	>11

3.2.2 HBU ZIRLO™ after RHT

Figure 11 shows offset strain vs. RCT test temperature for HBU ZIRLO™ following irradiation and following RHT at peak 400°C hoop stresses of 140 MPa and 110 MPa. The DBTT decreased from ≈185°C to ≈125°C for the decrease in RHT peak hoop stress from 140 MPa to 110 MPa.

Figure 12 compares the load-displacement curve for as-irradiated, HBU ZIRLO™ tested at 20°C to the one for HBU ZIRLO™ following RHT (400°C and 140 MPa peak hoop stress) and tested at 150°C. The first load drop for the RHT ring occurred during elastic loading at P = 220 N. After the load drop, loading increased at a linear rate to 270 N. Based on the >50% decrease in stiffness (i.e., loading slope), it was concluded that a crack had grown through >50% of the wall at the first load drop from 220 N. Thus, P_{max} = 220 N and δ_p/D_{mo} = 0% for the RHT sample. By contrast, RT results for as-irradiated ZIRLO™ were P_{max} = 570 N and δ_p/D_{mo} = 7.0%. The degradation in RCT properties due to RHT can be quantified as a 61% decrease in P_{max} and a ductility decrease from 7% to 0% for RCT temperatures below the DBTT. As with HBU M5®, quantification of P_{max} for samples that fail within the elastic regime requires a large number of tests because of the expected variation in P_{max} for the brittle failure mode. For the cladding ring following RHT, post-RCT examination indicted through-wall cracks at the 12 and 6 o'clock orientations. These cracks initiated at the cladding inner surface (location of maximum tensile hoop stress).

Figure 13 shows the hydride distribution and orientation in HBU ZIRLO™ in the as-irradiated condition (Fig. 13a), after RHT at a peak 400°C hoop stress of 140 MPa (Fig. 13b), and after RHT at a peak 400°C hoop stress of 110 MPa (Fig. 13c). For 140-MPa-RHT, continuous radial-circumferential hydrides precipitated during the 5°C/h cooling from 400°C. The longest pathway for continuous crack growth across the cladding wall was ≈80% of the wall thickness (see Fig. 13b), and the RHCF was 67±11% based on 16 images at two axial locations. For 110-MPa-RHT, the longest pathway for continuous crack growth across the cladding wall was ≈50% of the wall thickness (see Fig. 13c), and the RHCF was 30±12% based on 48 images at two axial locations.

Strength and ductility results from RCTs for as-irradiated ZIRLO™ and HBU ZIRLO™ following RHT are summarized in Table 7.

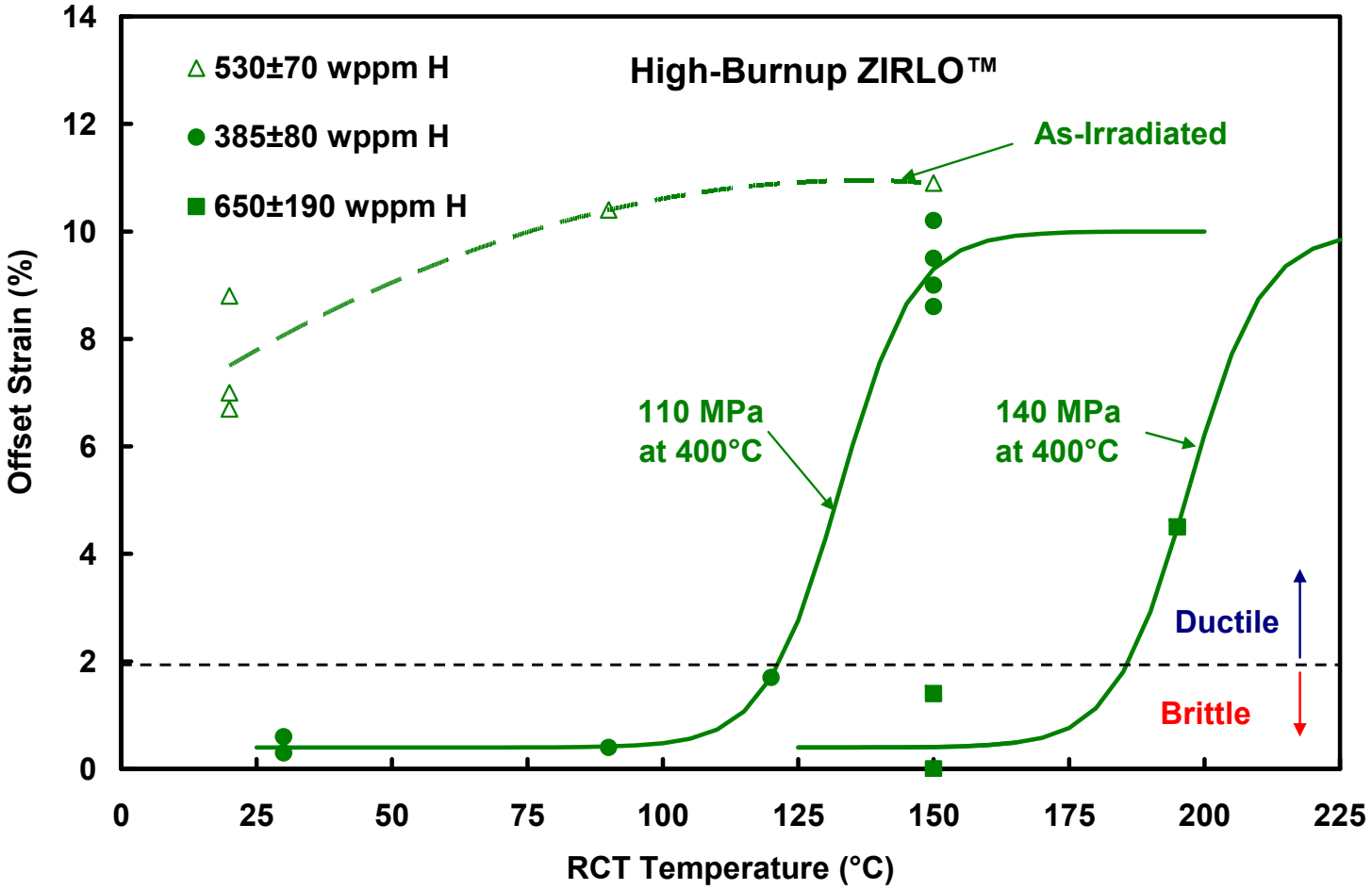

Figure 11. RCT offset strains vs. RCT temperature for HBU ZIRLO™ following irradiation and following RHT at peak 400°C hoop stresses of 140 MPa and 110 MPa.

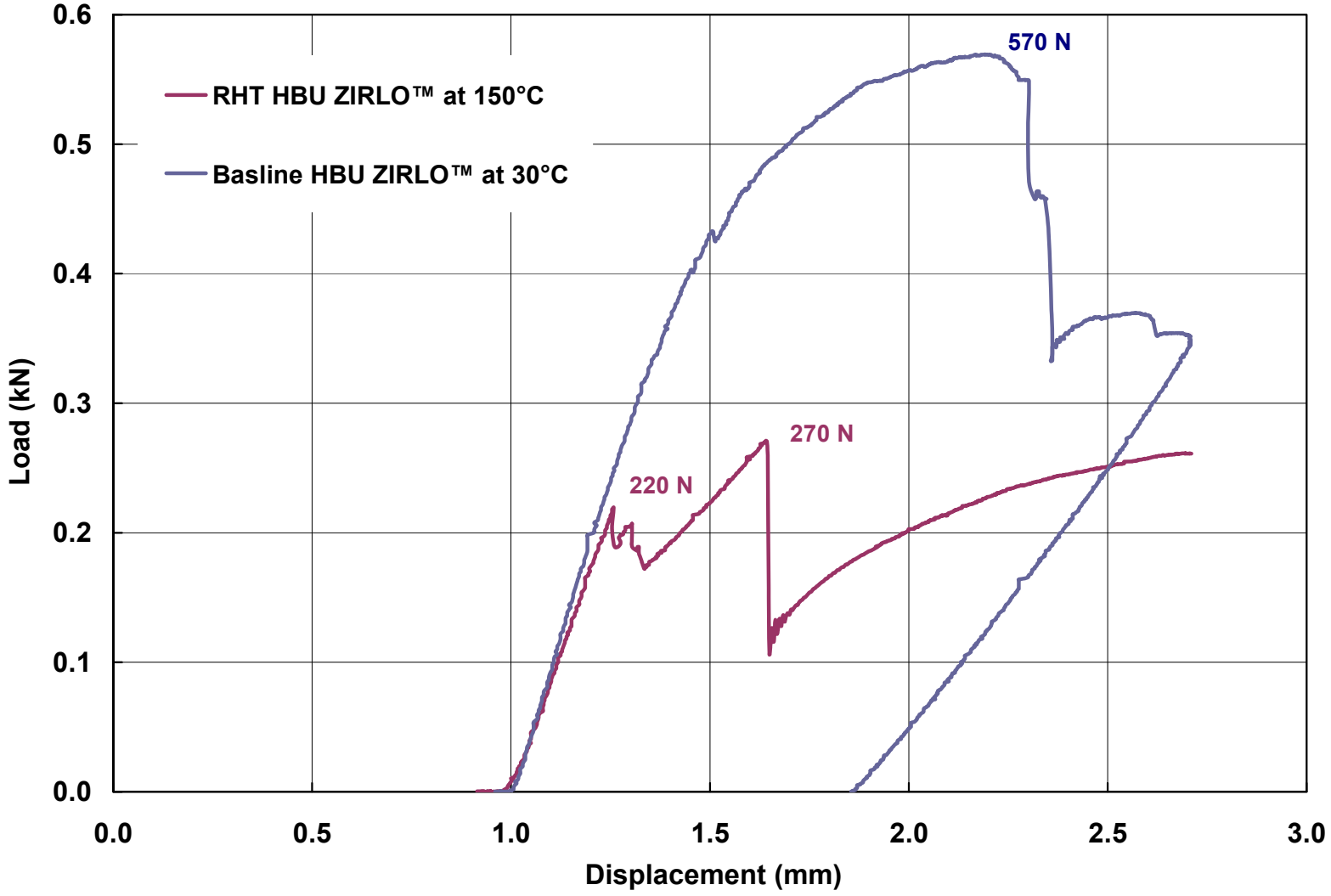

Figure 12. RCT load-displacement curves for HBU ZIRLO™: (a) as-irradiated (i.e., baseline) condition (see Fig. 13a) tested at 20°C and (b) following RHT at 400°C and 140 MPa (see Fig. 13b) and tested at 150°C.

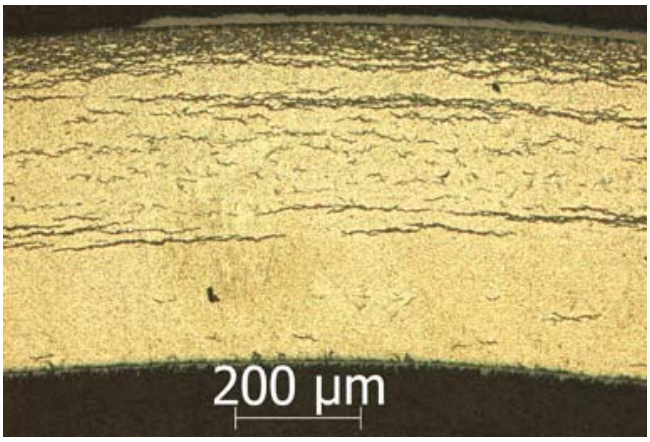

(a)

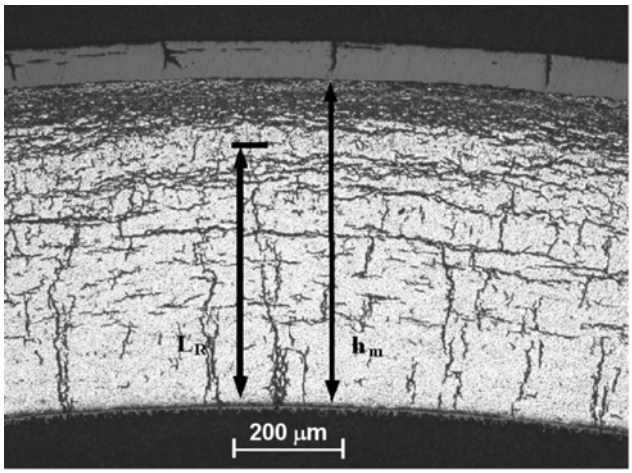

(b)

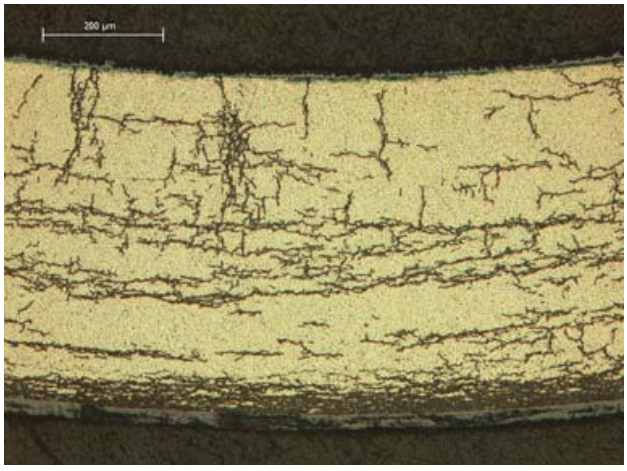

(c)

Figure 13. Hydride distribution and orientation in HBU ZIRLO™: (a) as-irradiated baseline with 530 wppm C_H, (b) after RHT at 400°C and 140 MPa with 650 wppm C_H, and (c) after RHT at 400°C and 110 MPa with 350 wppm C_H.

Table 7. Summary of strength (P_{max}) and ductility (δ_p/D_{mo}) results for HBU ZIRLO™ in the as-irradiated condition (i.e., baseline results) and following RHT. P_{max} was normalized to 8-mm sample length to determine the percentage decrease in maximum load relative to the baseline result (105A9).

Sample ID	Peak RHT T, °C	Peak RHT σ_θ, MPa	RCT T, °C	Reduction in P_{max}, %	Ductility δ_p/D_{mo}, %
105A9	---	---	20	0	7.0
648G5	400	140	150	61	0
648G10	400	140	150	17	1.4
648D3	400	110	30	40	0.6
648D5	400	110	150	9	>9.5
648D8	400	110	150	5	8.6
648D10	400	110	150	6	>9.0

3.2.3 HBU Zry-4 after RHT

Figure 14 shows offset strain vs. RCT test temperature for HBU Zry-4 following irradiation and following RHT at 400°C peak hoop stresses of 140 MPa and 110 MPa. The DBTT decreased from ≈55°C to <24°C for a decrease in RHT peak hoop stress from 140 MPa to 110 MPa. However, the gradual increase in ductility with increasing RCT temperature is not typical of a material that undergoes a ductile-to-brittle transition. The DBTT decrease may have been caused by the decrease in C_H (from 615±82 wppm to 520±90 wppm), as well as the decrease in RHCF (from 16±4% to 9±5%) resulting from the decrease in RHT peak hoop stress. This conjecture is supported by the embrittlement due to circumferential hydrides for as-irradiated HBU Zry-4 samples with 640±140 wppm. These as-irradiated samples were also brittle at 90°C.

Figure 15 compares the load-displacement curve for as-irradiated HBU Zry-4 (with 640±140 wppm) tested at 23°C to the one for HBU Zry-4 (with 615±82 wppm) following RHT (400°C and peak 140 MPa hoop stress) and tested at 30°C. The offset strains and maximum loads are comparable, but the extent of cracking is quite different following the first significant load drop. As shown in Fig. 16, a crack extending ≈40% through the wall was observed after a 27% load drop for as-irradiated HBU Zry-4. Following the 47% load drop shown in Fig. 15, deep cracks (≈90% of the wall) were observed at the 3 and 9 o'clock orientations at the ends of the as-irradiated ring. For the RHT ring, a 90% load drop is indicated in Fig. 15, and deep cracks were observed at the 3 (90%), 6 (50%), and 9 (70%) o'clock orientations at the ring ends.

Figure 16 shows the hydride distribution and orientation in HBU Zry-4 in the as-irradiated condition (Fig. 16a), after RHT at a 400°C peak hoop stress of 140 MPa (Fig. 16b), and after RHT at a peak 400°C hoop stress of 110 MPa (Fig. 16c). The radial hydrides in Figs. 16b and 16c are relatively short and located in positions across the wall such that they may have participated in crack propagation but not crack initiation in the dense hydride rim.

Strength and ductility results from RCTs for as-irradiated HBU Zry-4 and HBU Zry-4 following RHT are summarized in Table 8.

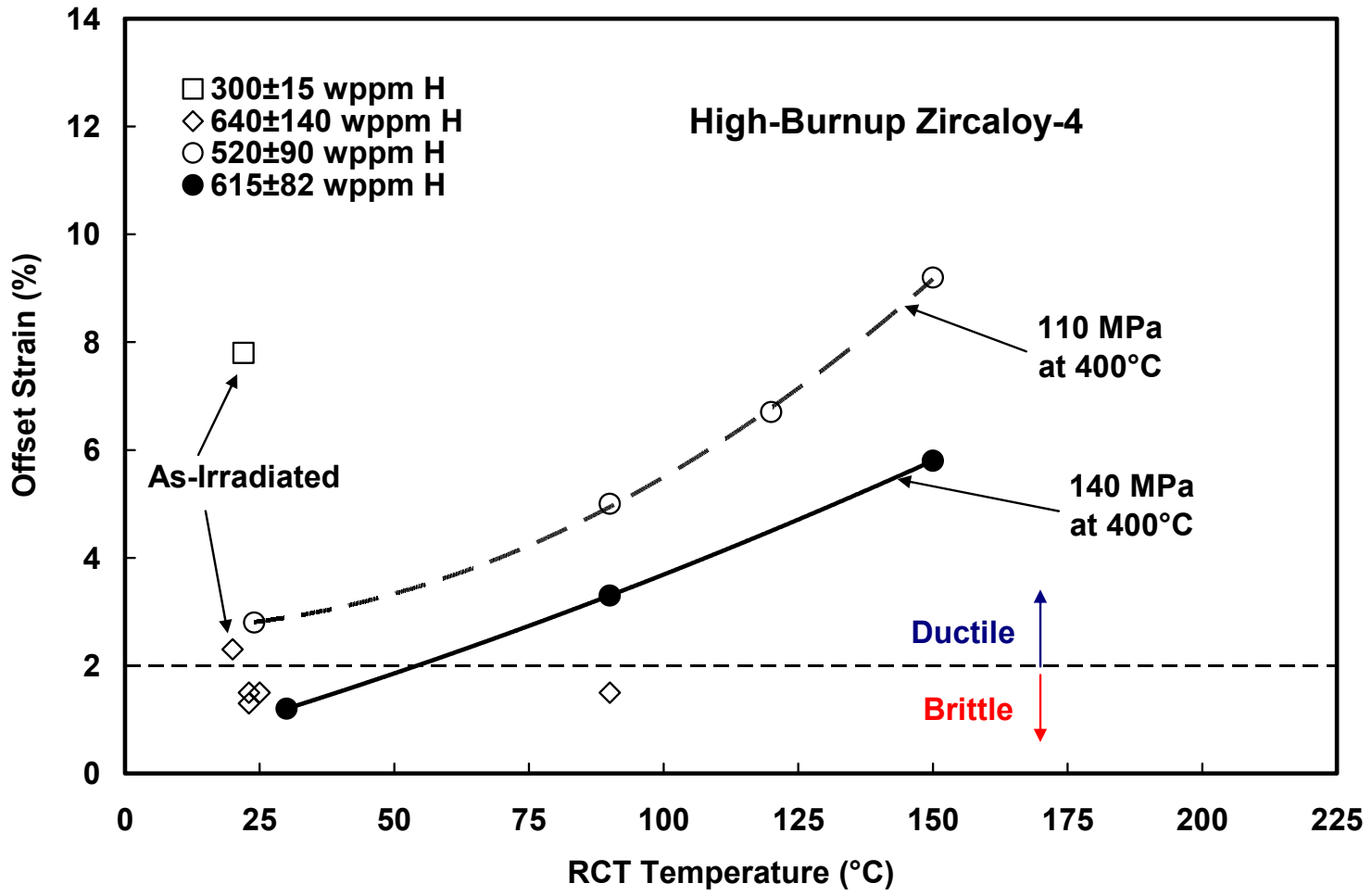

Figure 14. RCT offset strains vs. RCT temperature for HBU Zry-4 following irradiation and following RHT at peak 400°C hoop stresses of 140 MPa and 110 MPa.

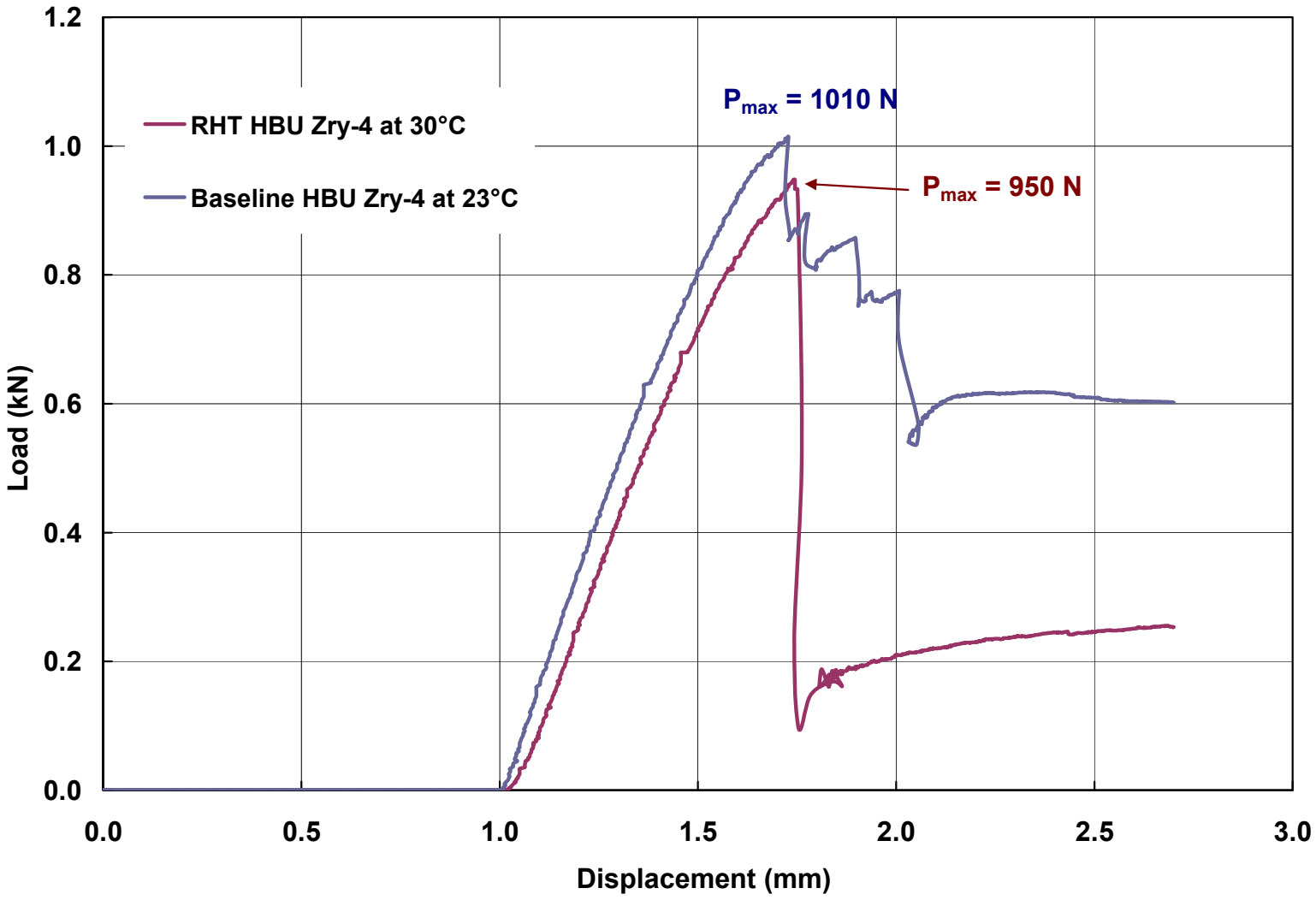

Figure 15. RCT load-displacement curves for HBU Zry-4: (a) as-irradiated (i.e., baseline) condition (see Fig. 16a) before drying-storage and tested at 23°C and (b) following RHT at 400°C and 140 MPa (see Fig. 16b) and tested at 30°C.

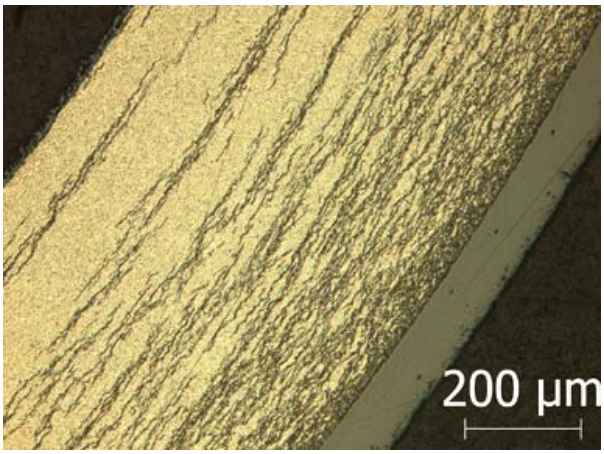

(a)

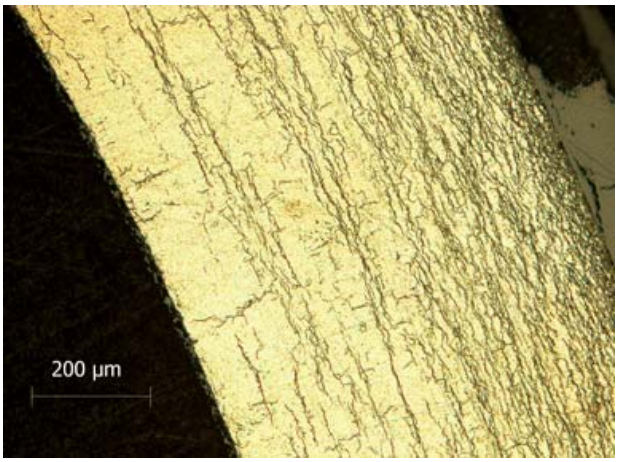

(b)

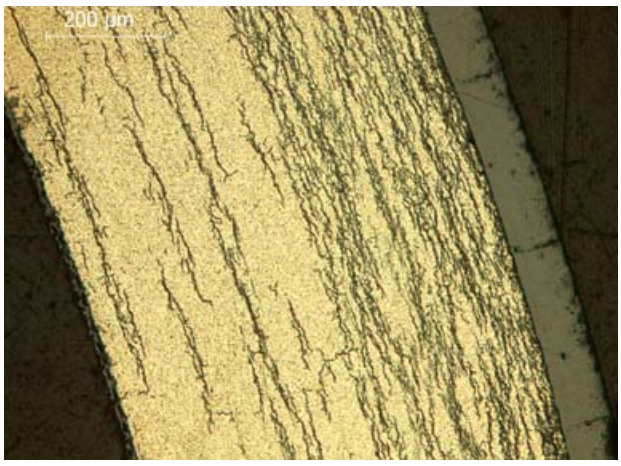

(c)

Figure 16. Hydride distribution and orientation in HBU Zry-4: (a) as-irradiated baseline with 640 wppm C_H, (b) after RHT at 400°C and 140 MPa with 615 wppm C_H, and (c) after RHT at 400°C and 110 MPa with 520 wppm C_H.

Table 8. Summary of strength (P_{max}) and ductility (δ_p/D_{mo}) results for HBU Zry-4 in the as-irradiated condition (i.e., baseline results) and following RHT. P_{max} was normalized to 8-mm sample length to determine the percentage decrease in maximum load relative to the baseline result (606C2J). Note-as-irradiated sample 605D3F2 had only 300 wppm C_H.

Sample ID	Peak RHT T, °C	Peak RHT σ_θ, MPa	RCT T, °C	Reduction in P_{max}, %	Ductility δ_p/D_{mo}, %
606C2J	–	–	23	0	1.5
605D3F2	–	–	22	-10	>9.9
605C2G	400	140	30	0.9	1.2
605C2F	400	140	90	14	3.3
605C2C	400	140	150	19	5.8
605C6E	400	110	24	6	2.8
605C6C	400	110	90	9	5.0
605C6J	400	110	120	22	6.7
605C6H	400	110	150	14	>9.2

4. CURRENT RESULTS

The peak RHT hoop stress was lowered to 90 MPa for HBU M5® and to 80 and 90 MPa for HBU ZIRLO™ in an effort to achieve the goal of DBTT ≤20°C. The peak RHT temperature (400°C) was maintained for these tests. For HBU M5®, the 90-MPa peak hoop stress was sufficient to clearly give DBTT <20°C. For HBU ZIRLO™, 80 MPa gave DBTT <20°C and 90 MPa gave 20°C DBTT. These results were for tests conducted with one-cycle heating-cooling (see Fig. 2). The 90-MPa RHT was repeated with two intermediate cooling (to 300°C) and heating (to 400°C) cycles to study the effects of multiple drying cycles on DBTT. The additional drying cycles did not cause an increase in radial-hydride precipitation (i.e., RHCF) or in DBTT. Detailed results for these tests are presented below.

4.1 HBU M5® Subjected to 400°C and 90 MPa Peak RHT Conditions

The segment (651E3) selected for this RHT was from the same HBU fuel rod from which the 110-MPa segment (651E5) originated. The axial locations of these two segments were 0.15 m apart with 651E3 below 651E5. Figure 17 shows the post-RHT sectioning diagram, along with C_H data, for the 90-MPa rodlet. Rings C, D, G and H were used for RCTs. Post-RCT hydrogen measurements were made for part of rings D and G. Ring F was used for pre-RHT metallographic examination. Post-RCT metallographic examination was performed for the mid-spans of rings D and G.

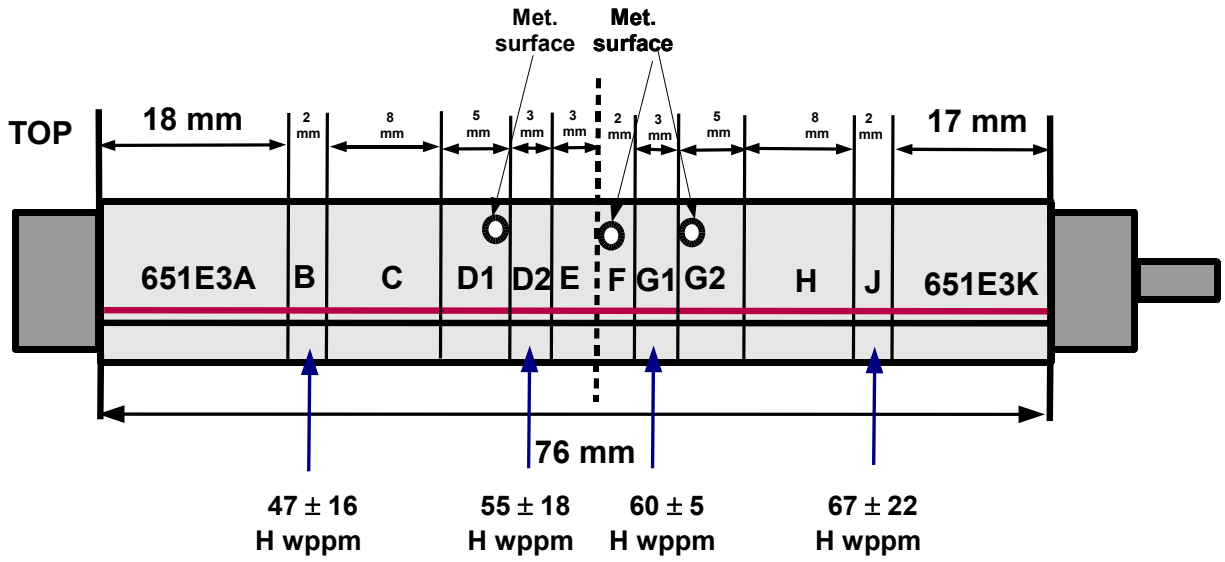

Figure 17. Sectioning diagram for HBU M5® rodlet subjected to 400°C RHT at 90-MPa peak stress.

Post-RHT characterization results for rodlet 651E3 were: D_o = 9.54±0.02 mm, h_{ox} = 9±1 μm, D_{mo} = 9.52±0.02 mm (based on 6 micrometer measurements), h_m = 0.56±0.01 mm (based on 12 metallographic images for ring F), C_H = 58±15 wppm (based on 12 data points with 0.75-g total mass), and RHCF = 31±15% (based on 54 metallographic images for rings D1, F, and G2). The results were comparable to rodlet 651E5 except that C_H was lower (58 wppm vs. 72 wppm) and RHCF was lower (31% vs. 61%) due to the decrease in peak RHT hoop stress.

Figure 18 contrasts radial hydrides in regions from rings 651E3F (90-MPa RHT) and 651E5C1 (110-MPa RHT). Radial hydride precipitation is extensive for both RHT hoop stresses. However, radial hydrides after 90-MPa RHT (Fig. 18a) tended to be shorter and disconnected from the inner surface as compared to radial hydrides precipitated after 110-MPa RHT (Fig. 18b). During RCT loading, radial hydrides emanating from the inner cladding surface are more damaging than radial hydrides located closer to the mid-wall.

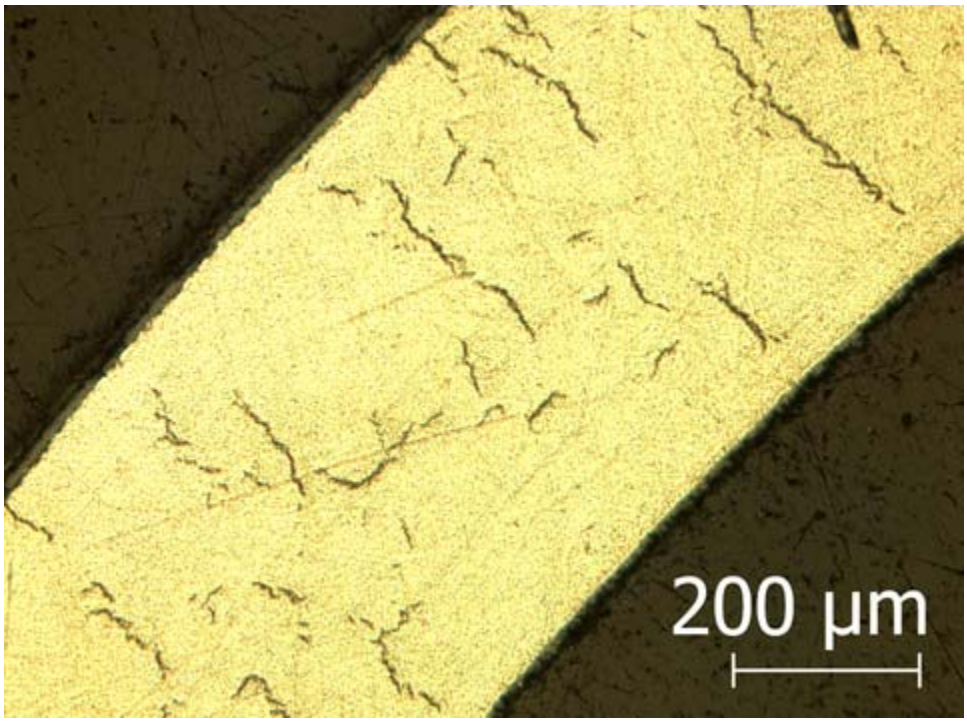

(a) 50% RHCF

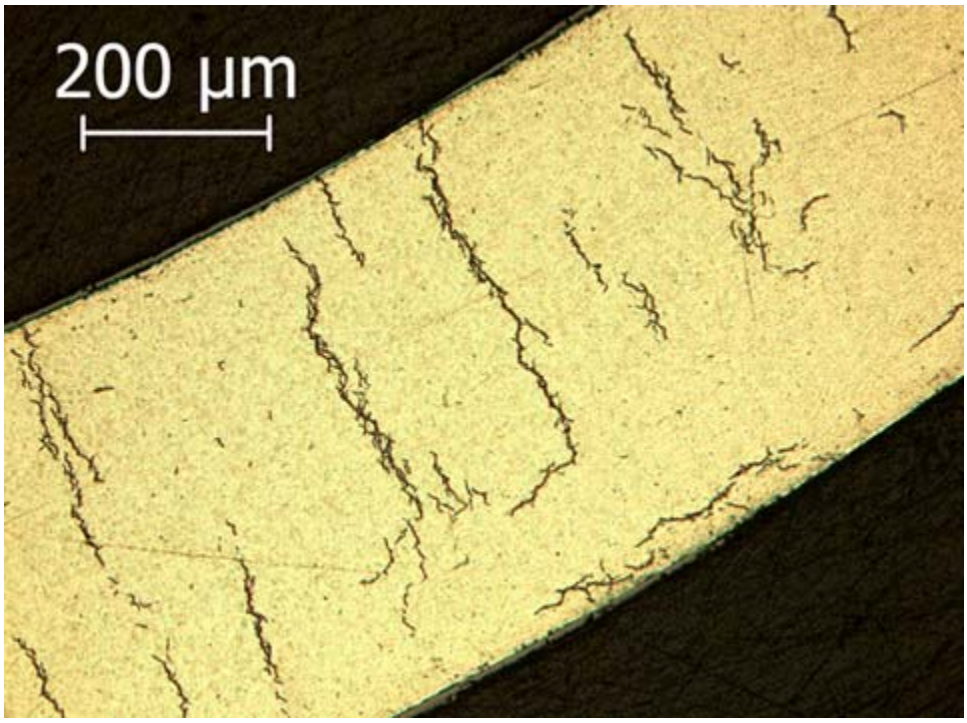

(b) 70% RHCF

Figure 18. RHCF values for HBU M5® rodlets subjected to 90-MPa (top) and 110-MPa (bottom) peak RHT hoop stresses: (a) 50% RHCF and (b) 70% RHCF.

RCTs were conducted at 23°C (rings G and D) and 60°C (rings C and H). Rings C and H had the same orientation with respect to the load at 12 o'clock. Rings C and H were rotated 90° prior to loading to study the effects of orientation on ductility. Recall that rings from the 110-MPa RHT rodlet were brittle at 30°C and 60°C while rings from the as-irradiated samples were highly ductile. Thus, emphasis was placed on conducting RCTs at ≤60°C for the 90-MPa RHT rodlet samples. Both rings tested at 23°C were ductile (8.7% and 10.5%). However, the ring oriented at the reference position (i.e., RCT load applied at the 12 o'clock orientation of the metallographic sample) experienced more extensive cracking (80% of wall at 12 o'clock and 87% of wall at 9 o'clock) than the ring rotated 90° prior to testing (75% of wall at 12 o'clock and 64% of wall at 6 o'clock). Rings tested at 60°C were fully ductile (no cracking) and had offset strains of 9.7%.

Load-displacement curves for these four RCTs are shown in Figs. 19 and 20. Figure 21 shows metallographic images of the dominant cracks formed at the 12 o'clock position (under the load) for the two rings tested at RT.

Table 9 compares characterization and ductility results from the rodlets subjected to 90-MPa (651E3) and 110-MPa (651E5) peak hoop stress at 400°C. These results are plotted in Fig. 22, along with results from as-irradiated HBU M5® and HBU M5® subjected to 140-MPa RHT. Ductility results for the 90-MPa RHT rings were about the same as those for as-irradiated cladding even though the RHT cladding had radial hydrides that were about 30% of the wall thickness.

The ductility at ≤60°C of rings sectioned from the HBU M5® rodlet subjected to 90-MPa peak RHT stress was significantly higher than the ductility of rings from the rodlet subjected to 110-MPa peak RHT stress. It is not clear how much of this improvement was due to the lower stress and how much was due to the lower average C_H. Based on the data generated to date, the DBTT of HBU M5® is <20°C for peak RHT hoop stresses ≤90 MPa. However, a test is planned for an M5® rodlet with ≈70 wppm C_H subjected to 100-MPa peak RHT hoop stress to enable distinction between the benefits of lower C_H and of lower hoop stress.

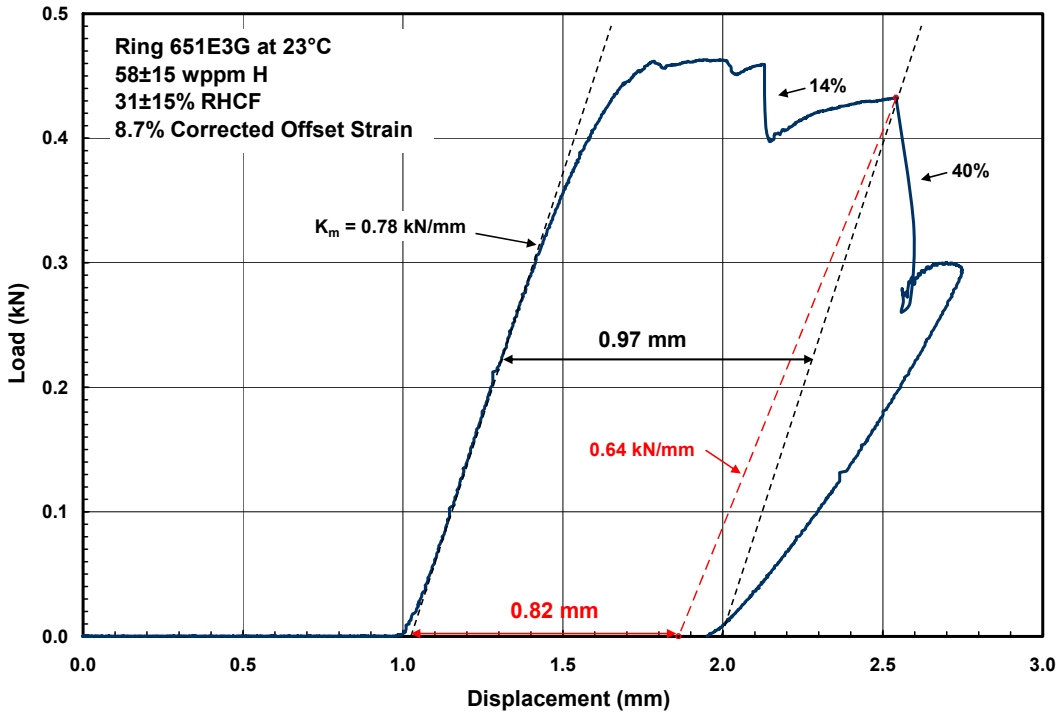

(a)

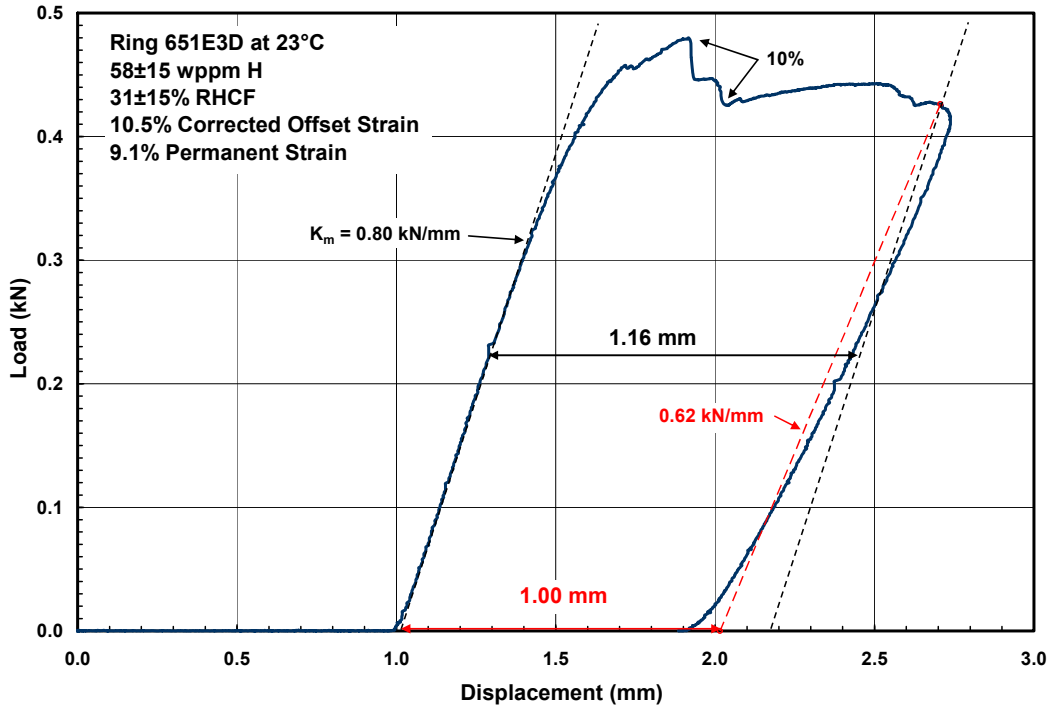

(b)

Figure 19. Load-displacement curves for RCTs conducted at 23°C with two samples from the HBU M5® rodlet subjected to 90-MPa peak hoop stress at 400°C: (a) reference orientation and (b) rotation of 90° prior to loading.

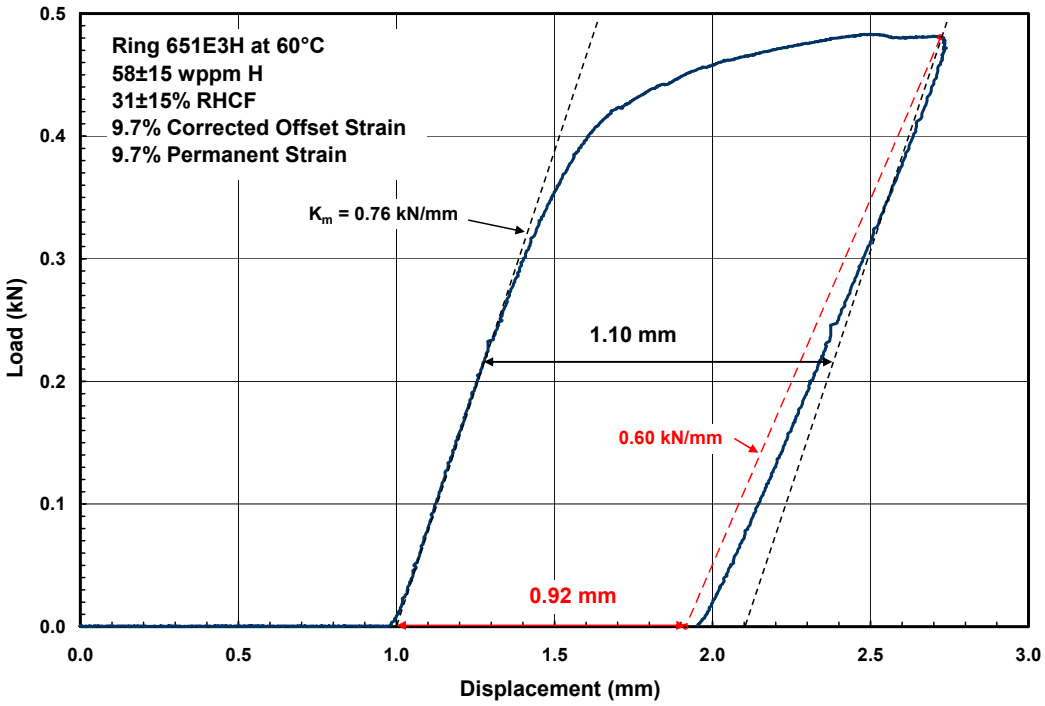

(a)

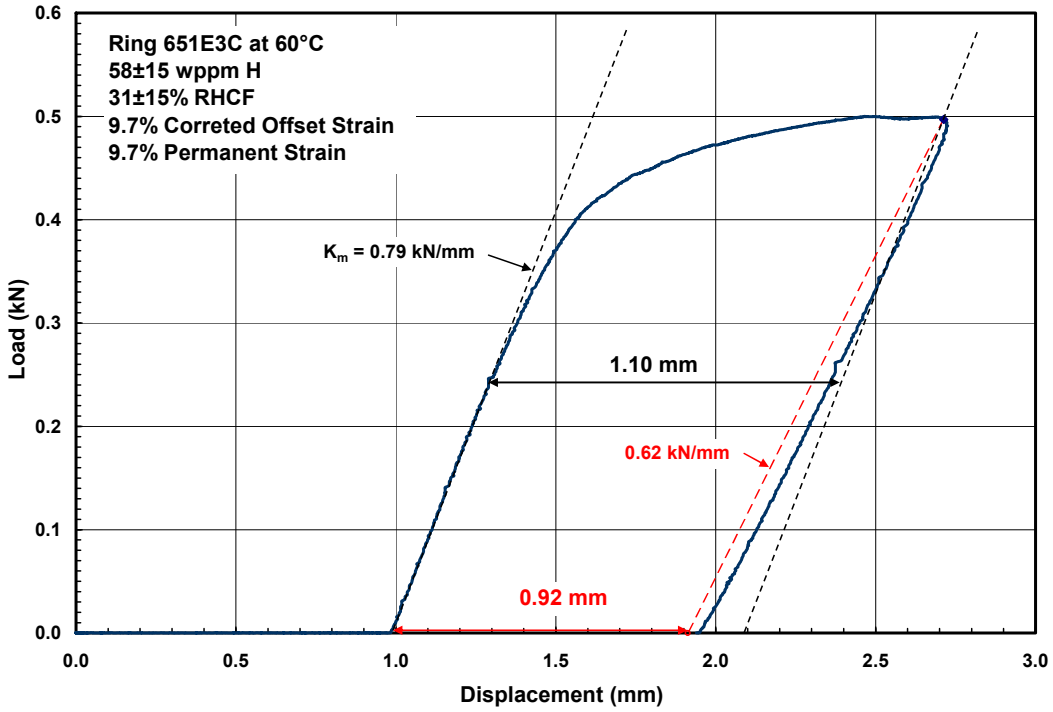

(b)

Figure 20. Load-displacement curves for RCTs conducted at 60°C with two samples from the HBU M5® rodlet subjected to 90-MPa peak hoop stress at 400°C: (a) reference orientation and (b) rotation of 90° prior to loading.

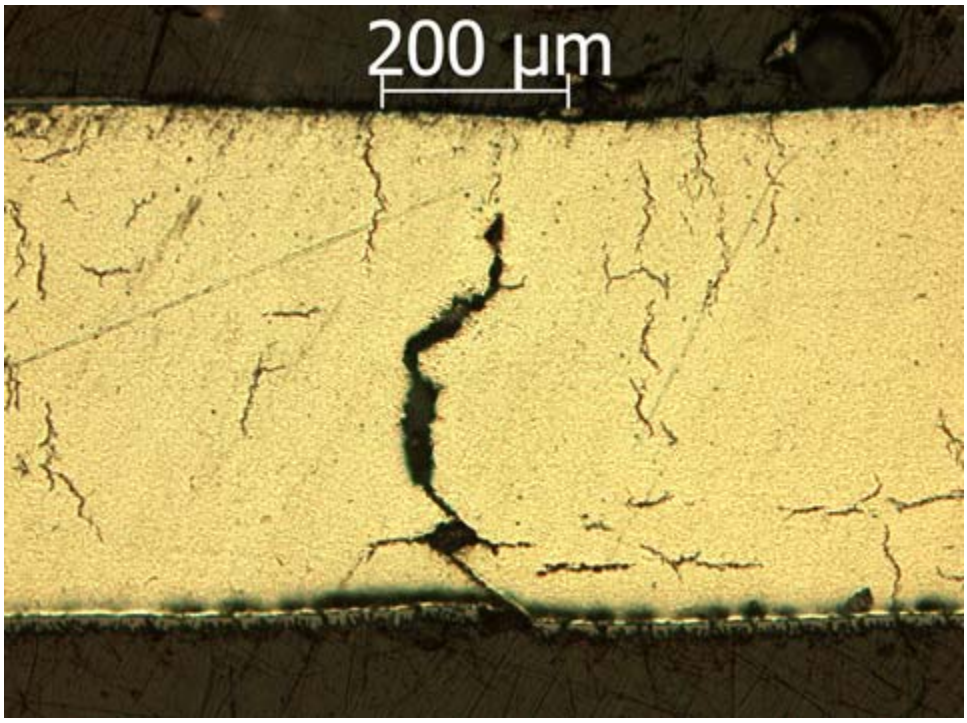

(a)

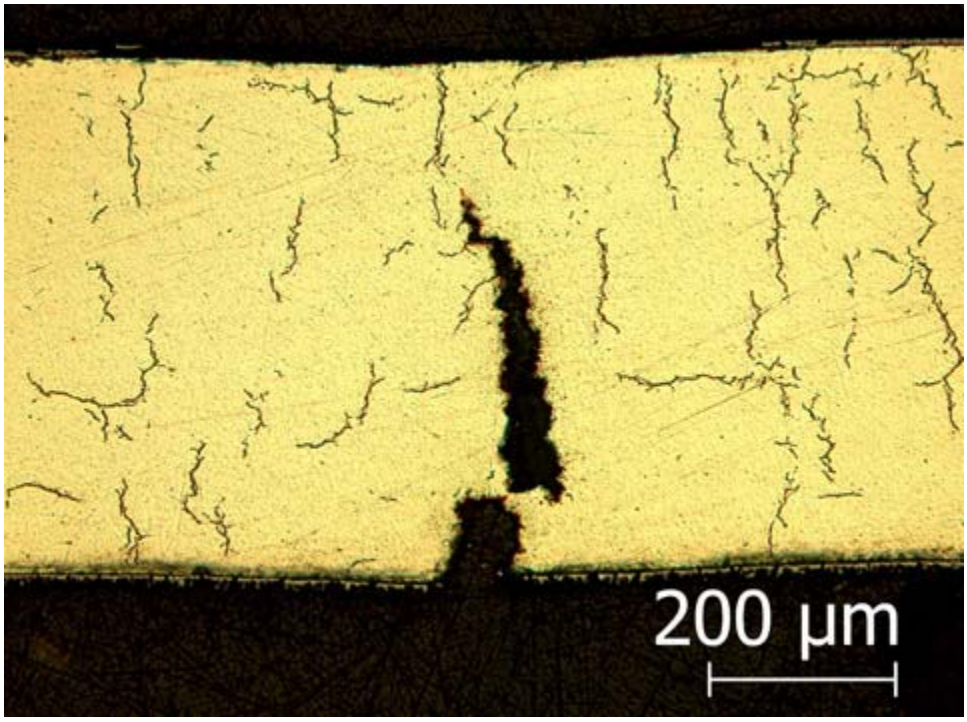

(b)

Figure 21. Major cracks observed following RCTs at 23°C and 5 mm/s displacement rate: (a) ring G with reference orientation and (b) ring D, which was rotated 90° prior to loading.

Table 9. Comparison of characterization and ductility for HBU M5® rodlets subjected to 90-MPa and 110-MPa hoop stress at 400°C prior to cooling at 5°C/h.

Parameter	Rodlet 651E3 90-MPa RHT	Rodlet 651E3 110-MPa RHT
Hydrogen Content, wppm	58±15	72±10
Radial-hydride Continuity Factor, %	31±15	61±10
Ductility at RT, %	8.7, 10.5	1.4 (brittle)
Ductility at 60°C, %	>9.7, >9.7	1.1 (brittle)
Ductility at 90°C, %	–	>10.9
DBTT, °C	<20	70

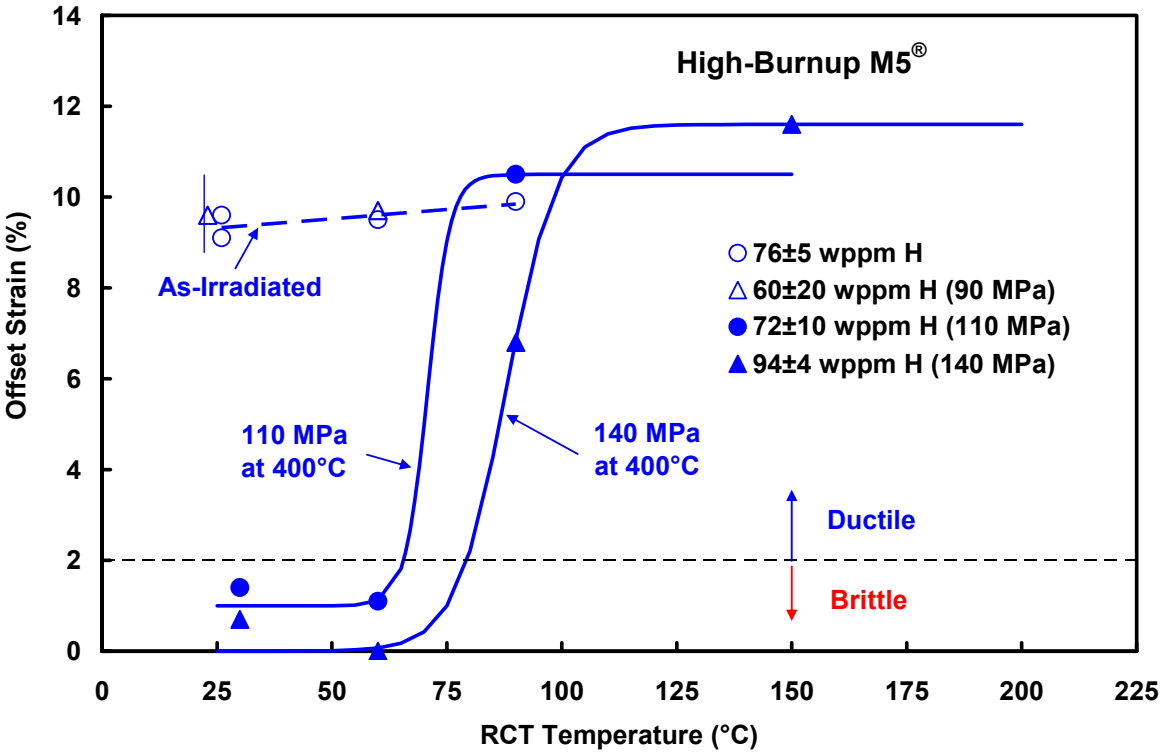

Figure 22. Ductility data and DBTT for as-irradiated HBU M5® and HBU M5® subjected to peak RHT hoop stresses of 90, 110, and 140 MPa at 400°C prior to cooling at 5°C/h. The 90-MPa RHT results are indistinguishable from ductility results for as-irradiated cladding.

4.2 HBU ZIRLO™ Subjected to 80-90 MPa Peak RHT Stress at 400°C

Segments 105B and 105C were selected for RHT of HBU ZIRLO™ at peak 400°C RHT hoop stresses of 80 and 90 MPa, respectively. These segments were from the same HBU fuel rod from which the as-irradiated segment (105A) was sectioned. The three segments were contiguous with 105B just above 105A and 105C just above 105B. Figures 23 and 24 show post-RHT sectioning diagrams, along with C_H data, for 80-MPa and 90-MPa rodlets. Post-RHT characterization results are summarized in Table 10.

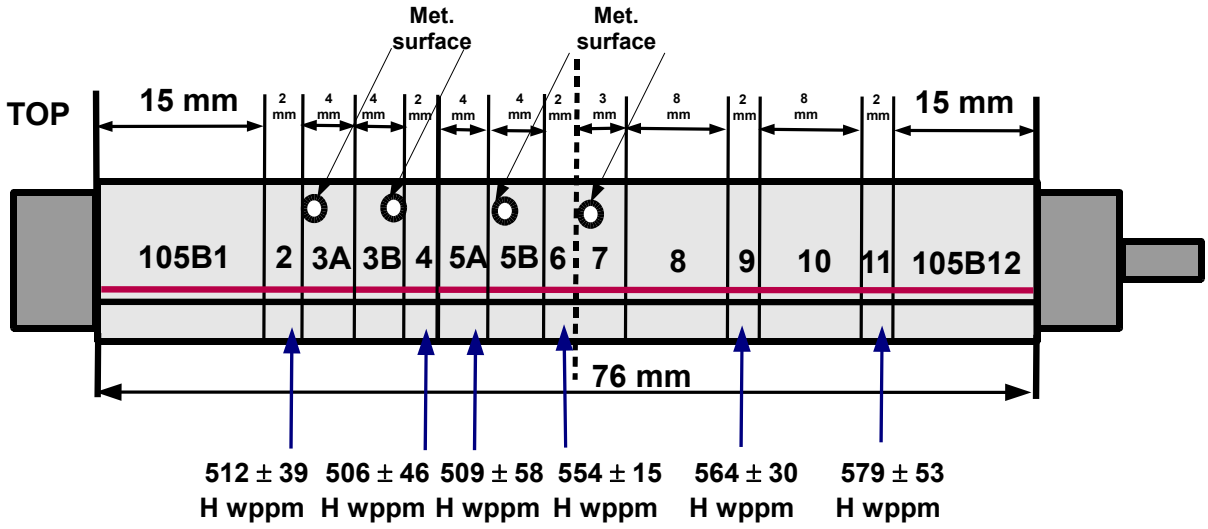

Figure 23. Sectioning diagram for HBU ZIRLO™ rodlet subjected to 400°C RHT at 80 MPa.

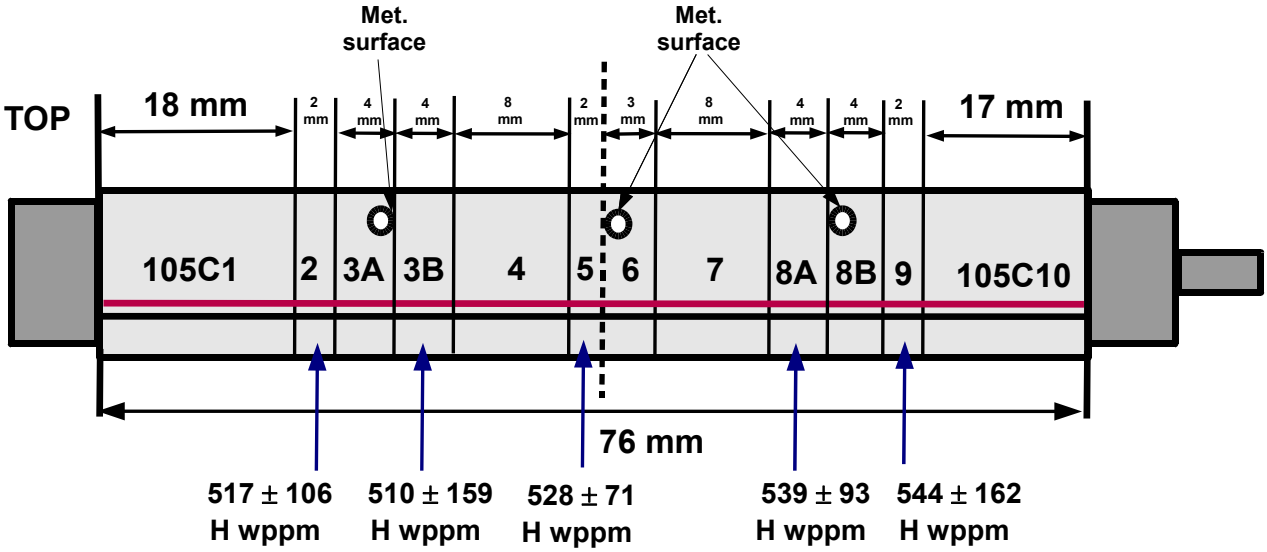

Figure 24. Sectioning diagram for HBU ZIRLO™ rodlet subjected to 400°C RHT at 90 MPa.

Table 10. Post-RHT characterization results for HBU ZIRLO™ rodlets subjected to 80-MPa (105B) and 90-MPa (105C) peak hoop stresses at 400°C prior to cooling at 5°C/h.

Parameter	Rodlet 105B 80-MPa RHT	Rodlet 105C 90-MPa RHT
Outer Diameter (D_o), mm	9.54±0.02	9.53±0.02
Oxide Layer Thickness (h_{ox}), μm	48±3	47±3
Metal Outer Diameter (D_{mo}), mm	9.44±0.02	9.44±0.02
Metal Wall Thickness (h_m), mm	0.54±0.00	0.55±0.01
Hydrogen Content (C_H), wppm	535±50	530±115
Radial-hydride Continuity Factor (RHCF), %	9±3	19±9

The geometrical parameters, as well as the average C_H values, are quite similar for the two rodlets. Thus, a direct comparison can be made on the effects of the two peak RHT hoop stress values. Combining these results with those presented in Section 3.2.2, it is clear that the reduction in peak RHT hoop stress had a significant effect on RHCT, which was 30±12% for 110 MPa, 19±9% for 90 MPa and 9±3% for 80 MPa.

Figure 25 contrasts radial hydrides in regions from rings 105C6 (90-MPa RHT) and 105B7 (80-MPa RHT). The longest effective radial hydride (RHCF) in the 105C6 sector (Fig. 25a) is 36% of the cladding wall thickness, which is close to the maximum length observed for the three cross sections examined. The longest radial hydride (7% of wall thickness) shown in Fig. 24b is close to the average RHCF for that rodlet. However, it is shown because it was one of the few radial hydrides observed to extend to the cladding inner surface.

RCT results for the two rodlets are given in Table 11. From these results, it is clear that the DBTT is <20°C for the lower RHT stress (80 MPa) and 20°C for the higher RHT stress (90 MPa). These results, along with ductility results for as-irradiated ZIRLO™ and ZIRLO™ subjected to RHT at 140-MPa and 110-MPa peak hoop stresses, are plotted in Fig. 26. Following Fig. 26 are plots of the load-displacement curves for rings from the rodlets with 90-MPa and 80-MPa peak hoop stress (Figs. 27-30).

Figure 31 shows post-RHT metallographic results for dominant cracks formed in rings from 90-MPa and 80-MPa peak hoop stress rodlets. For the higher-stress (90 MPa) rodlet with 19±9% RHCF, dominant cracks initiated at the cladding inner surface at the 12 and/or 6 o'clock orientations due to the presence of radial hydrides (see Fig. 31a). However, post-RCT results for rings with only 9±4% RHCF (80-MPa RHT rings) clearly support the contention that radial hydrides did not contribute to crack initiation in these samples. Cracks that developed in these rings were similar to those observed in as-irradiated rings in that they initiated at the outer cladding surface at the 3 and/or 9 o'clock orientations due to the high density of circumferential hydrides and the high tensile stresses at these locations (see Fig. 31b). These shorter radial hydrides may have participated in crack propagation.

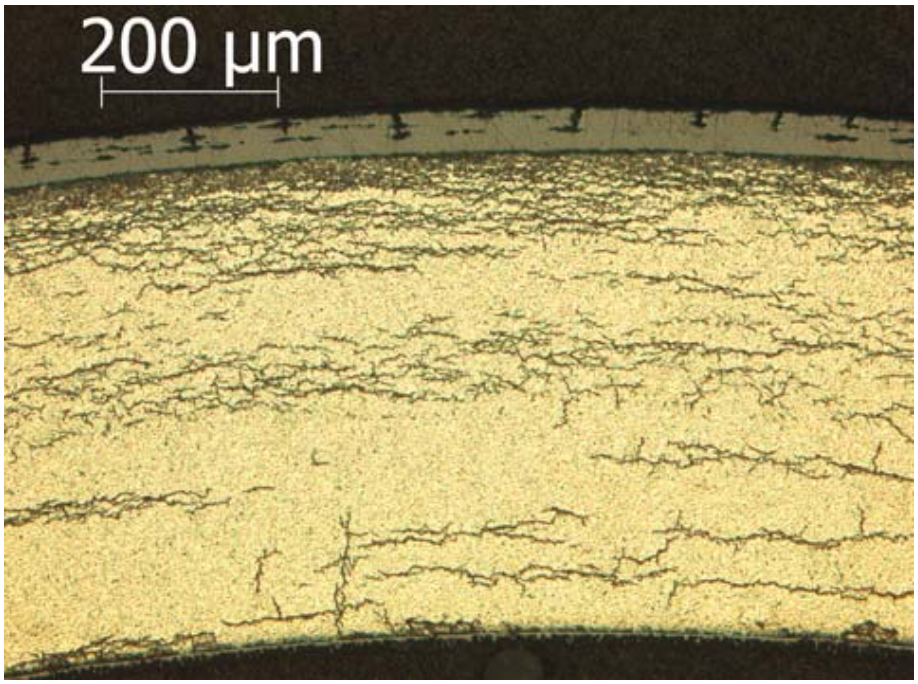

(a) 36% RHCF

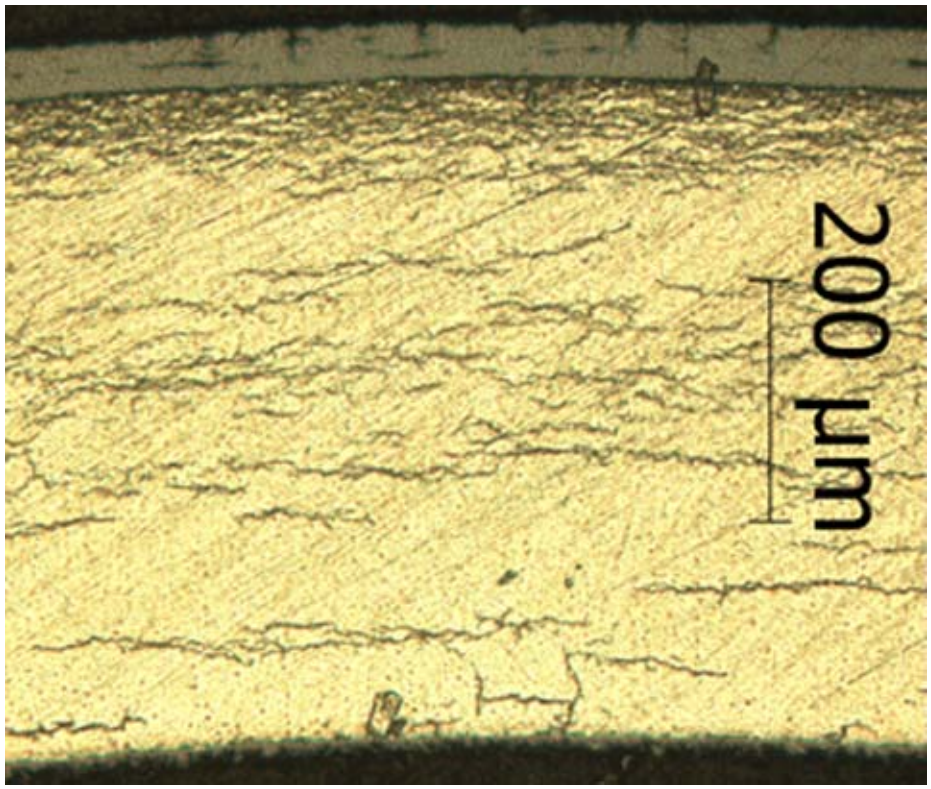

(b) 7% RHCF

Figure 25. RHCF values for HBU ZIRLO™ rodlets subjected to 90-MPa (top) and 80-MPa (bottom) peak RHT hoop stresses at 400°C: (a) 36% RHCF and (b) 7% RHCF.

Table 11. Comparison of characterization and ductility for HBU ZIRLO™ rodlets subjected to peak RHT hoop stresses of 90 MPa and 80 MPa at 400°C prior to cooling at 5°C/h.

Parameter	Rodlet 105C 90-MPa RHT	Rodlet 105B 80-MPa RHT
Hydrogen Content, wppm	530±115	535±50
Radial-hydride Continuity Factor, %	19±9	9±4
Ductility at 23°C, %	2.2	5.3
Ductility at 60°C, %	7.2	5.7
Ductility at 90°C, %	>10.6	>9.5
Ductility at 120°C, %	>10.6	–
Ductility at 150°C, %	–	>10.1
DBTT, °C	20	<20

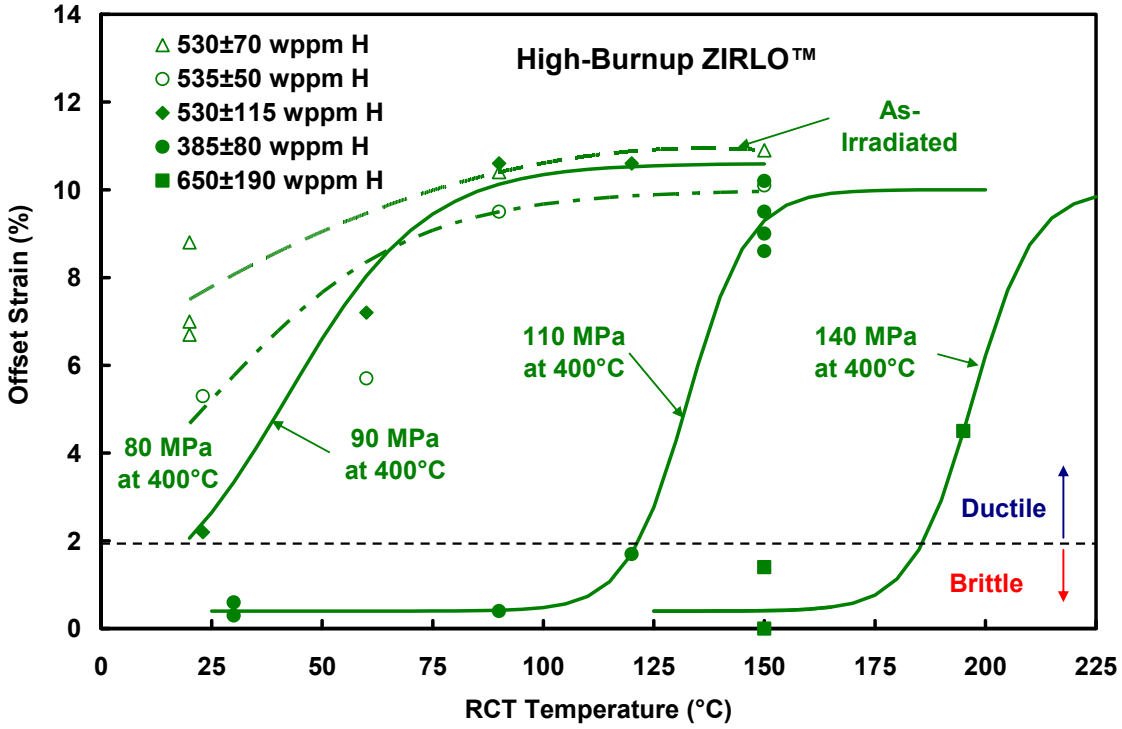

Figure 26. Ductility data and DBTT for as-irradiated HBU ZIRLO™ and HBU ZIRLO™ subjected to peak RHT hoop stresses of 80, 90, 110, and 140 MPa at 400°C prior to cooling at 5°C/h.

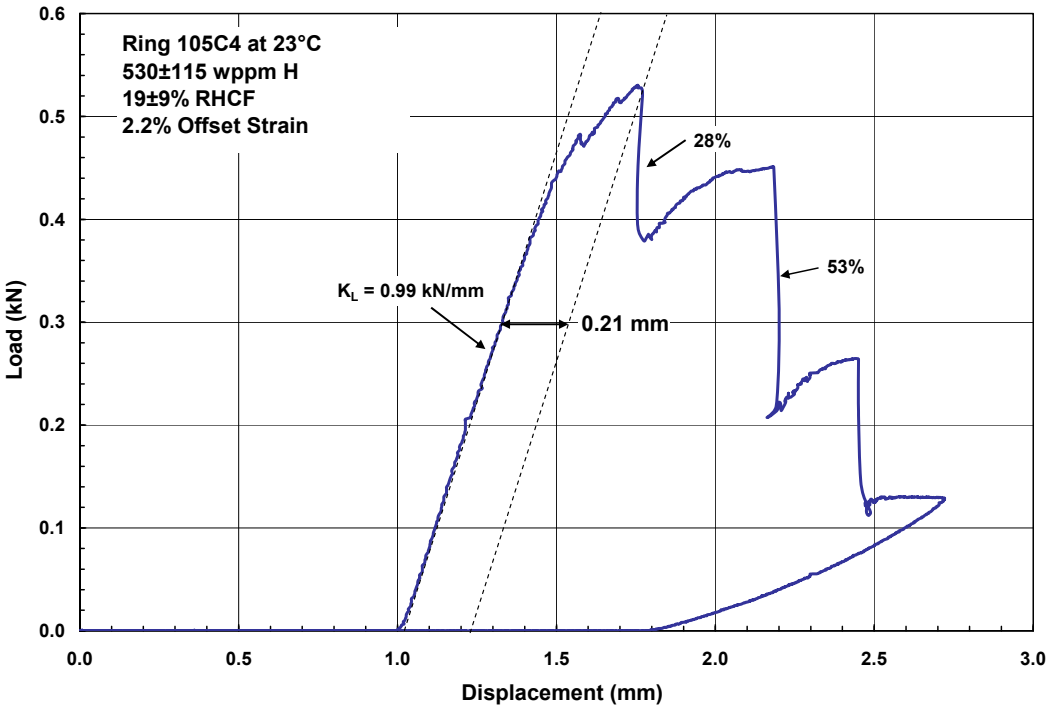

(a) 90 MPa

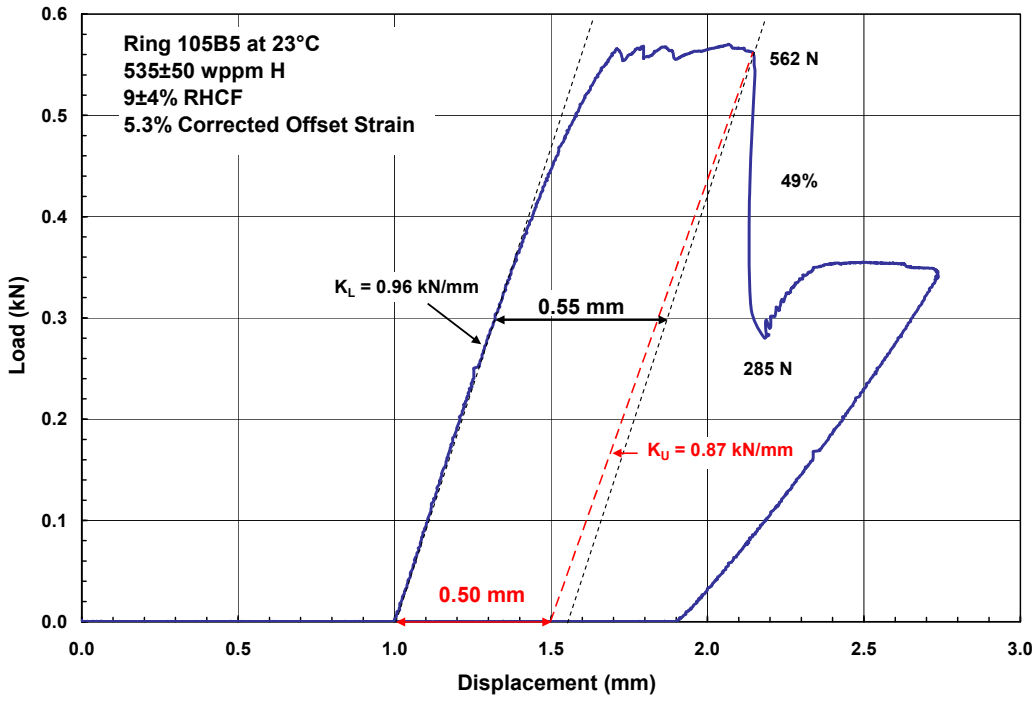

(b) 80 MPa

Figure 27. Load-displacement curves for RCTs conducted at 23°C with samples from HBU ZIRLO™ rodlets subjected to RHT at 400°C hoop stresses of: (a) 90 MPa and (b) 80 MPa.

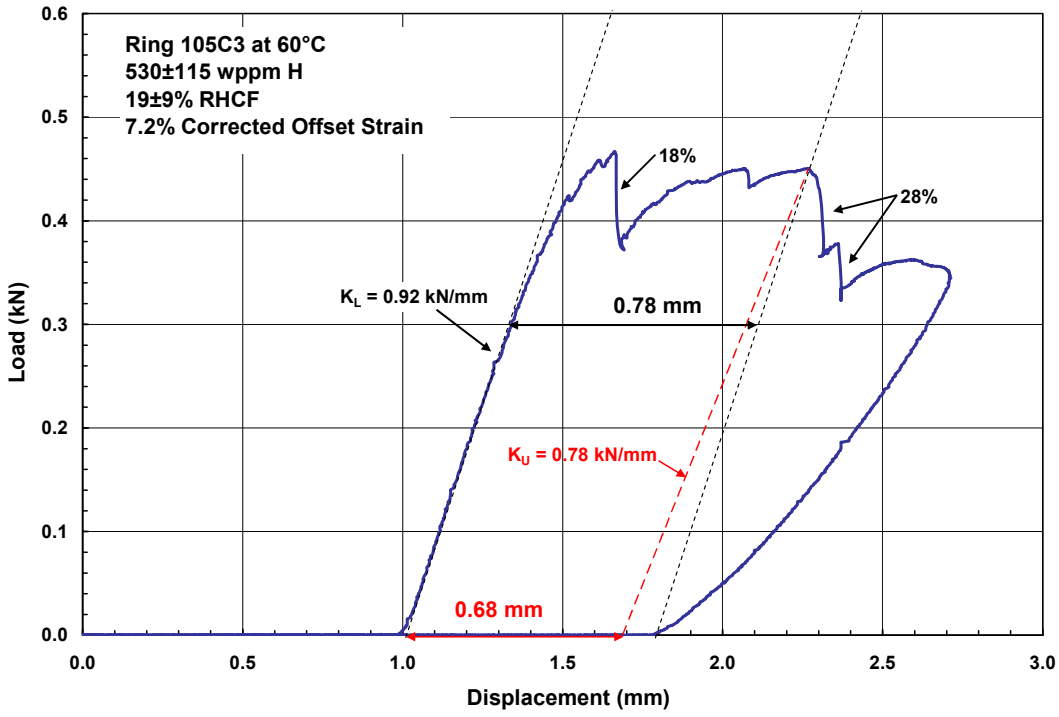

(a) 90 MPa

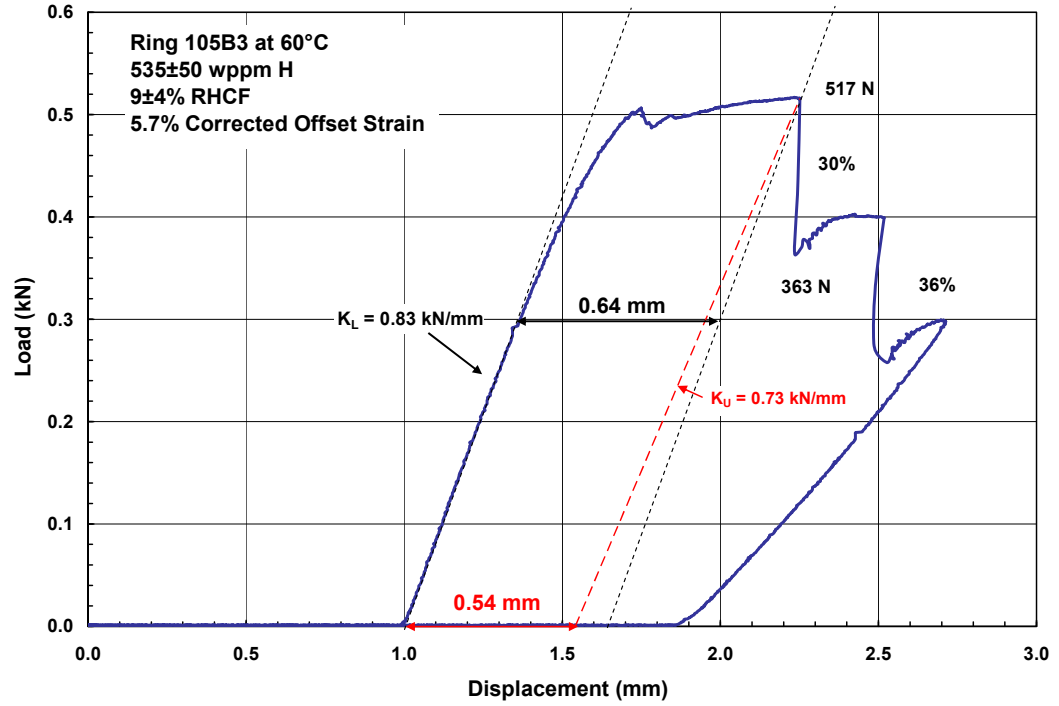

(b) 80 MPa

Figure 28. Load-displacement curves for RCTs conducted at 60°C with samples from HBU ZIRLO™ rodlets subjected to RHT at 400°C hoop stresses of: (a) 90 MPa and (b) 80 MPa.

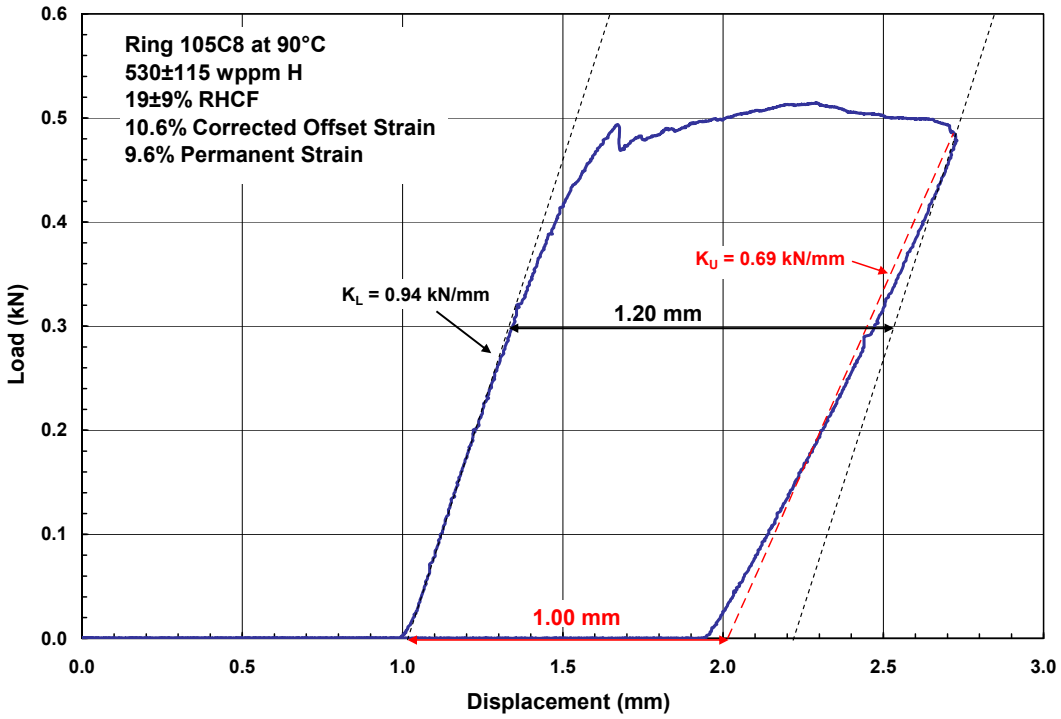

(a) 90 MPa

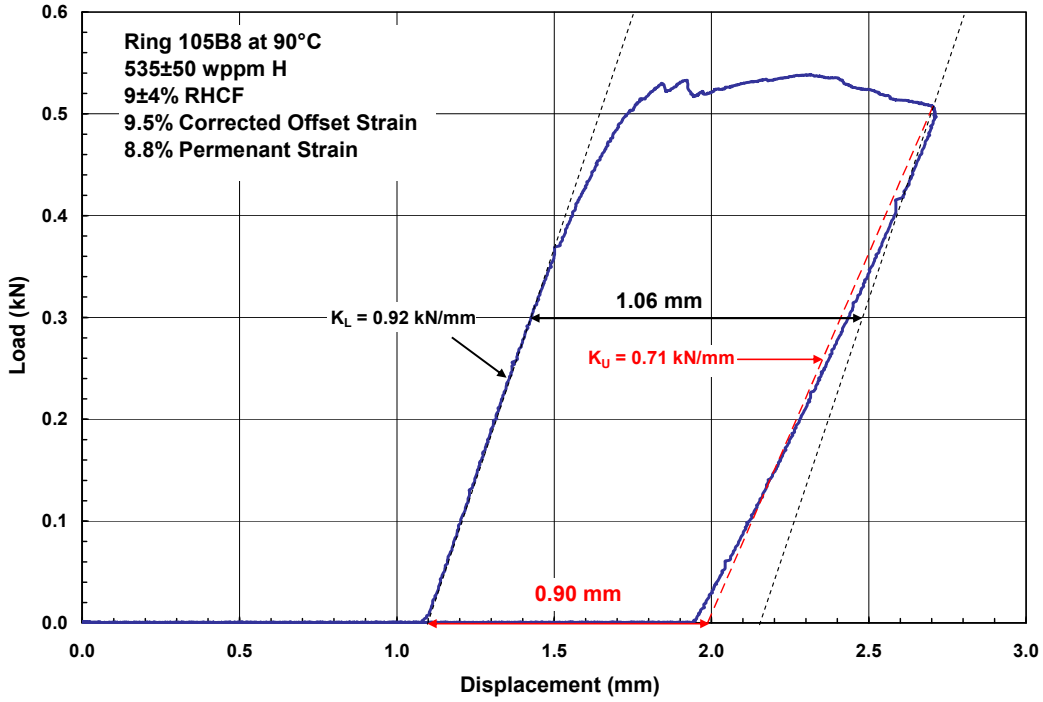

(b) 80 MPa

Figure 29. Load-displacement curves for RCTs conducted at 90°C with samples from HBU ZIRLO™ rodlets subjected to RHT at 400°C hoop stresses of: (a) 90 MPa and (b) 80 MPa.

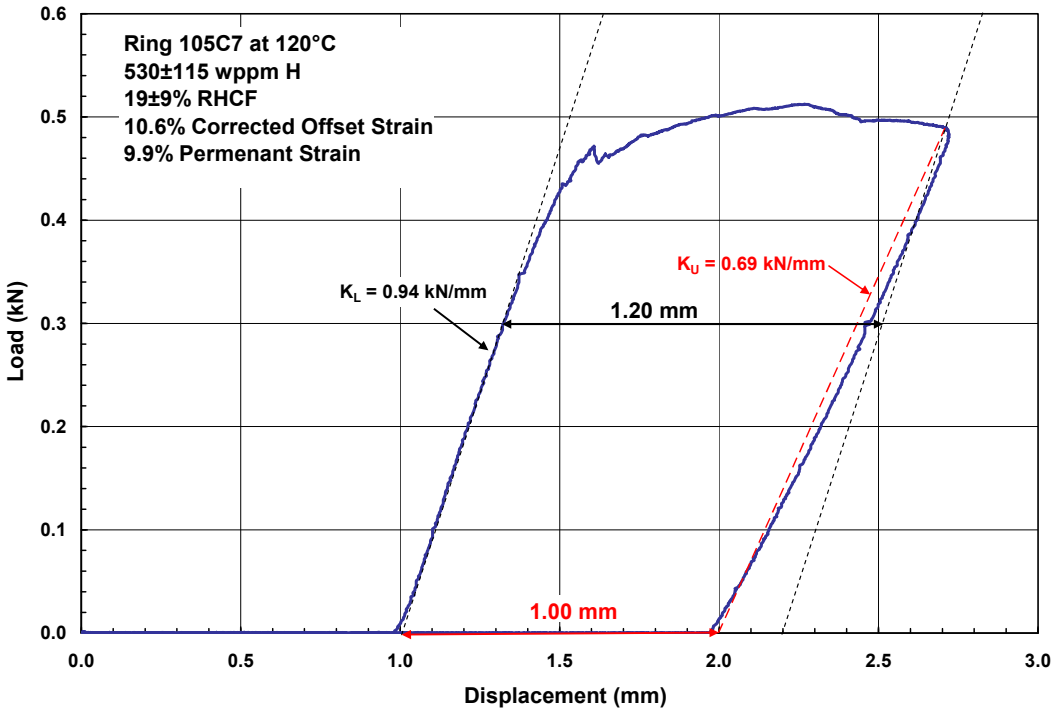

(a) 90-MPa RHT and 120°C RCT

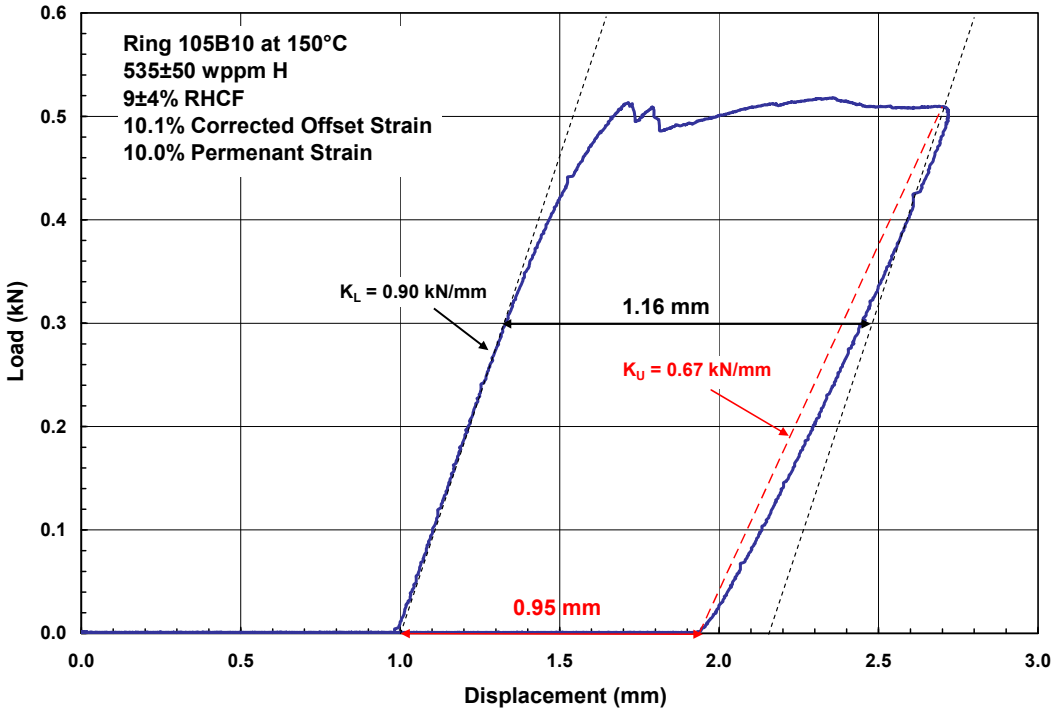

(b) 80-MPa RHT and 150°C RCT

Figure 30. Load-displacement curves for RCTs conducted with samples from HBU ZIRLO™ rodlets subjected to RHT at 400°C: (a) 90-MPa and 120°C RCT and (b) 80-MPa RHT and 150°C RCT.

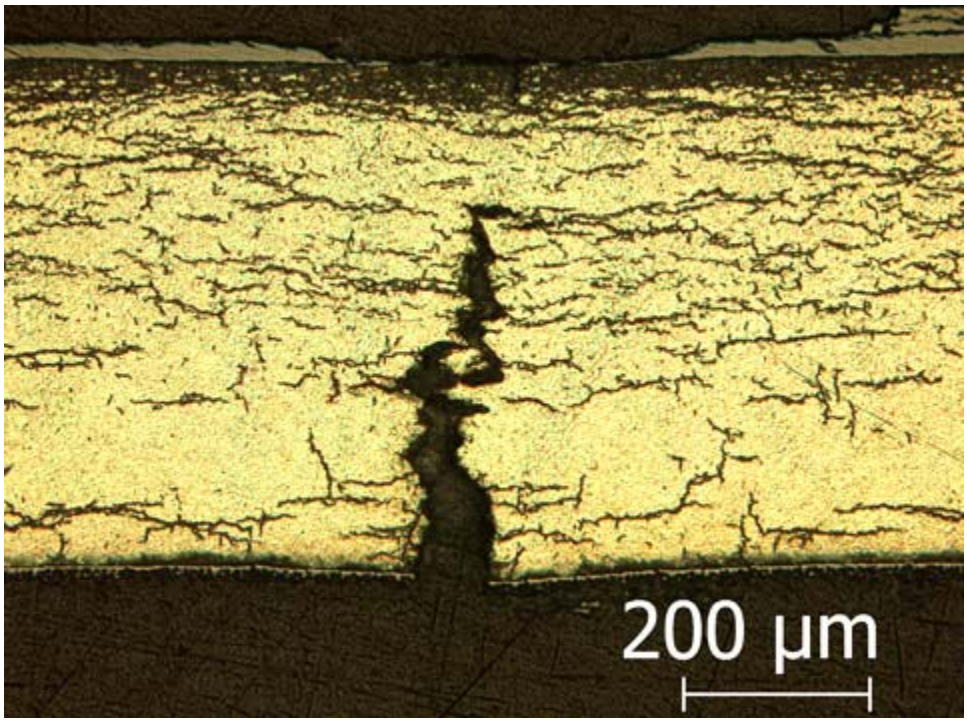

(a) 90-MPa RHT ring at 12 o'clock

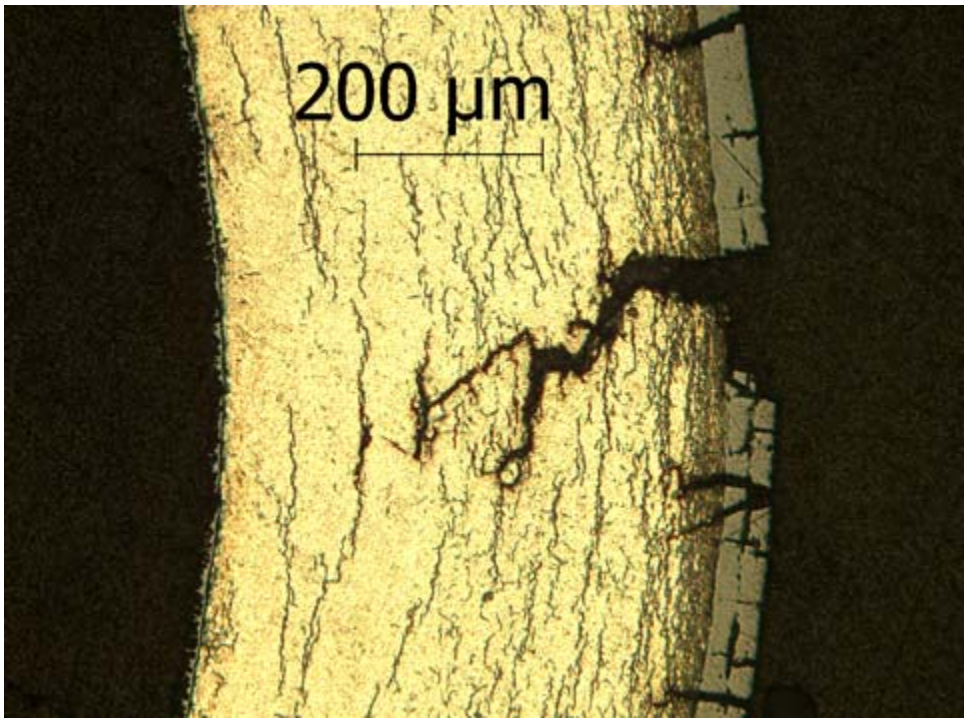

(b) 80-MPa RHT ring at 3 o'clock

Figure 31. Major cracks observed in HBU ZIRLO™ following RCTs at 60°C and 5 mm/s displacement rate: (a) 90-MPa RHT ring at 12 o'clock and (b) 80-MPa RHT ring at 3 o'clock.

4.3 HBU ZIRLO™ Subjected to Multiple Drying Cycles

Segment 105D was selected for multiple-drying-cycle RHT of HBU ZIRLO™ at peak 400°C RHT hoop stress of 90 MPa. This segment was from the same HBU fuel rod from which the single-cycle 105C was sectioned and was just above the 105C segment. Both segments were subjected to the same peak RHT stress of 90 MPa at 400°C. This approach allowed a direct assessment of the effects of temperature cycling on the DBTT. Previous studies with non-irradiated, pre-hydrided Zry-4 indicated a significant increase in radial hydride length and number density with an increasing number of temperature cycles (ΔT = 100°C and an increase from 1 to 4 cycles) at high hoop stress (150 MPa) [11]. These tests were conducted with uniformly pre-hydrided Zry-4. They were also conducted under conditions of constant hoop stress during cooling. However, it is not clear form these tests with uniformly pre-hydrided cladding whether the same degradation would be observed in HBU cladding (highly non-uniform C_H across the wall) that was cooled at a lower peak stress level with stress allowed to decrease during cooling.

The temperature history for the multiple-drying-cycle test had the same initial heating ramp and final cooling ramp as was used for segment 105C (see Fig. 2). However, two intermediate cooling-heating cycles were added with ΔT = 100°C, one-hour hold times, and 5°C/h cooling rates. Figure 32 shows the post-RHT sectioning diagram, along with measured values for C_H, for rodlet 105D.

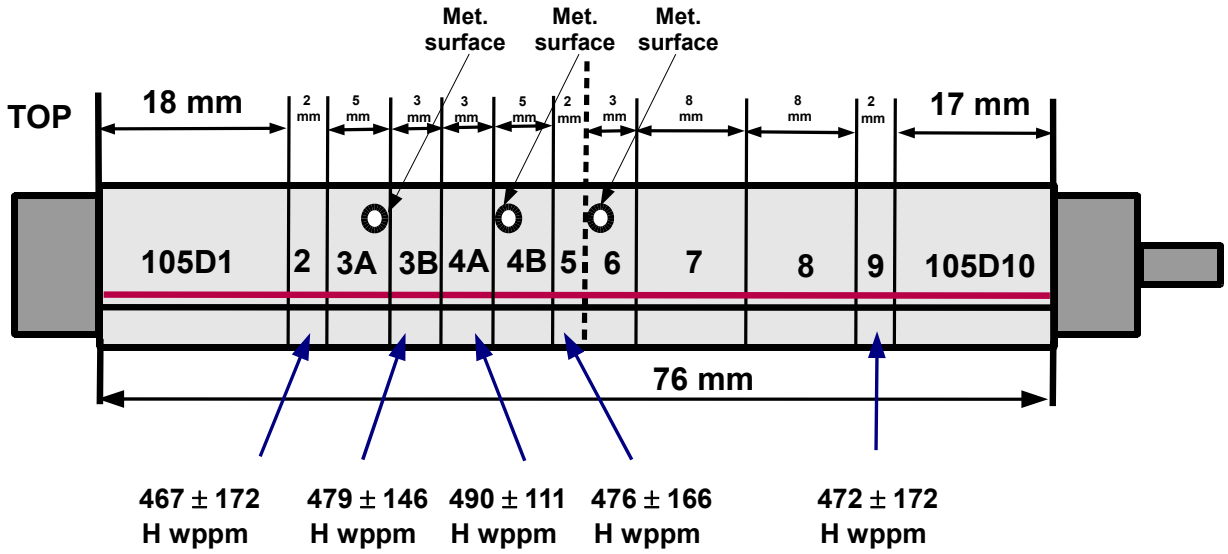

Figure 32. Sectioning diagram for HBU ZIRLO™ rodlet 105D subjected to 400°C RHT at 90 MPa peak hoop stress with two intermediate cooling-heating cycles (ΔT = 100°C).

Post-RHT characterization results are given in Table 12 for rodlet 105D and compared to those measured for 105C. The geometrical parameters are quite similar for the two rodlets. The corrosion layer thickness (40 µm vs. 47 µm) and average C_H (480 wppm vs. 530 wppm) were both lower than values obtained for rodlet 105C. However, neither of these parameters is expected to have a significant effect on radial hydride precipitation. Also, the average C_H difference (50 wppm) between these two rodlets is much less than the one-sigma values reflecting circumferential and axial variations within each rodlet. These variations within a rodlet and from rodlet to rodlet were due to variations in hydride rim thickness. The hydride distribution and number density below the hydride rim were comparable for both rodlets. The most significant characterization result in Table 12 is the RHCF, which is essentially the same (about 20%) for both rodlets. This result alone suggests no significant effects of multiple drying cycles on radial hydride precipitation, RCT ductility vs. temperature, or DBTT.

Table 12. Post-RHT characterization results for HBU ZIRLO™ rodlets subjected to 80-MPa (105B) and 90-MPa (105C) peak hoop stresses at 400°C prior to cooling at 5°C/h.

Parameter	Rodlet 105D 90-MPa RHT 3-Cycle-Cooling	Rodlet 105C 90-MPa RHT 1-Cycle-Cooling
Outer Diameter (D_o), mm	9.53±0.01	9.53±0.02
Oxide Layer Thickness (h_{ox}), µm	40±5	47±3
Metal Outer Diameter (D_{mo}), mm	9.45±0.01	9.44±0.02
Metal Wall Thickness (h_m), mm	0.56±0.01	0.55±0.01
Hydrogen Content (C_H), wppm	480±131	530±115
Radial-hydride Continuity Factor (RHCF), %	20±9	19±9

Figure 33 shows the similarities between the longest radial hydrides (36% RHCF) precipitated in rodlet 105D cladding as compared to the longest radial hydrides (36% RHCF) precipitated in rodlet 105C6 cladding. While previous micrographs presented in this report are from 100X images, Fig. 33 micrographs are from 200X images to allow a more detailed comparison between hydride morphologies.

RCT results for the two rodlets are given in Table 13. From these results, it is clear that the previous results obtained for 1-cycle cooling (20°C DBTT) also apply to 3-cycle cooling at the same peak RHT hoop stress (90 MPa). These results are compared graphically in Fig. 34. Following Fig. 34 are plots of the load-displacement curves for rings sectioned from 3-cycle cooling rodlet (Figs. 35 and 36).

In the non-linear displacement regime, an abrupt load drop >25% has been shown to correlate with unstable crack growth through >50% of the cladding wall. However, it is also possible to have stable (i.e., slower) crack growth without an abrupt load drop. For HBU ZIRLO™ tested at 60°C (Fig. 35b), the load increases to about 400 N and with the exception of minor load drops remains at about 400 N until the large load drop occurs. The maximum load achieved in the 90°C test was 540 N for a ring of comparable length (7.95 mm vs. 7.83 mm). Thus, cracking does occur during the 60°C test prior to the precipitous load drop at 9.4% corrected offset strain. The number and depth of cracks that form prior to 9.4% offset strain are not clear. However, it is possible that the offset strain prior to >50% wall crack is <9% for the RCT conducted at 60°C.

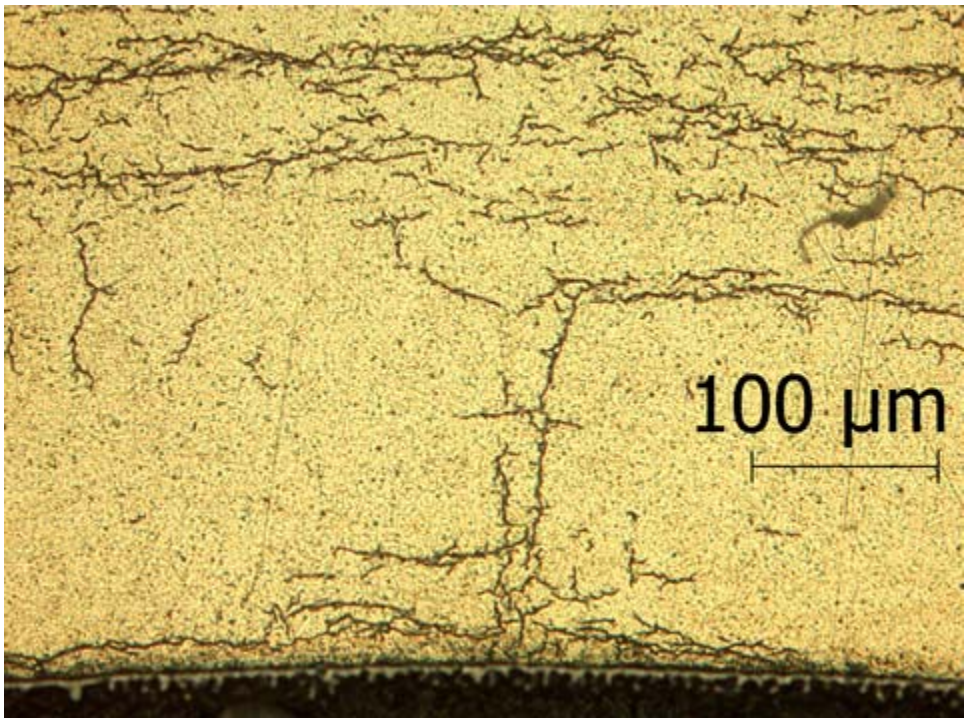

(a) 36% RHCF for 1-cycle cooling

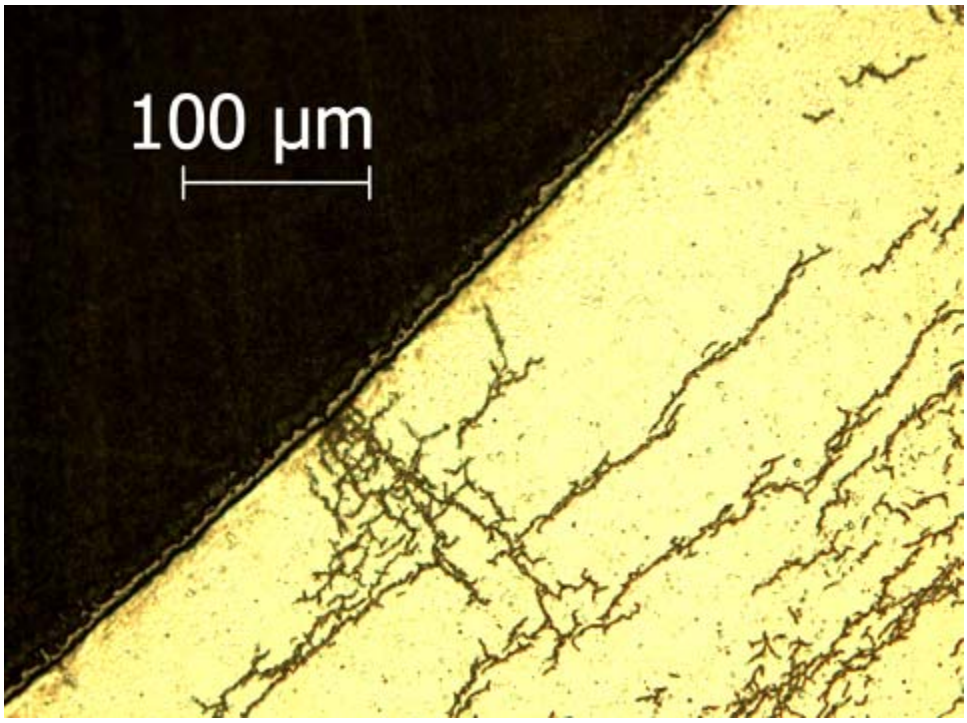

(b) 36% RHCF for 3-cycle cooling

Figure 33. RHCF values for HBU ZIRLO™ rodlets subjected to 90-MPa peak RHT hoop stress at 400°C: (a) 36% RHCF for 1-cycle cooling and (b) 36% RHCF for 3-cycle cooling.

Table 13. Comparison of characterization and ductility for HBU ZIRLO™ rodlets subjected 3-cycle (105D) and to 1-cycle (105C) cooling at a peak RHT hoop stress of 90 MPa at 400°C.

Parameter	3-Cycle Cooling Rodlet 105D 90-MPa RHT	1-Cycle Cooling Rodlet 105C 90-MPa RHT
Hydrogen Content, wppm	480±131	530±115
Radial-hydride Continuity Factor, %	20±9	19±9
Ductility at RT, %	2.6 (26°C)	2.2 (23°C)
Ductility at 60°C, %	9.4	7.2
Ductility at 90°C, %	>10.6	>10.6
Ductility at 120°C, %	>10.2	>10.6
DBTT, °C	20	20

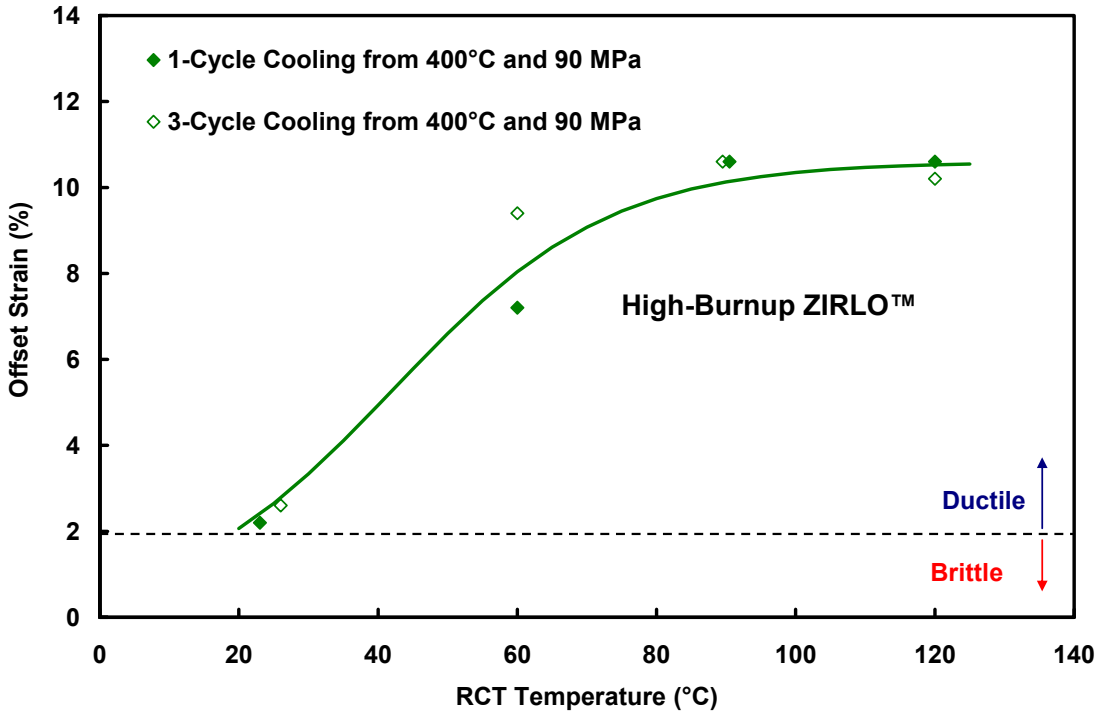

Figure 34. Ductility data and DBTT for HBU ZIRLO™ subjected to 1-cycle and 3-cycle cooling at 90-MPa peak RHT hoop stress at 400°C.

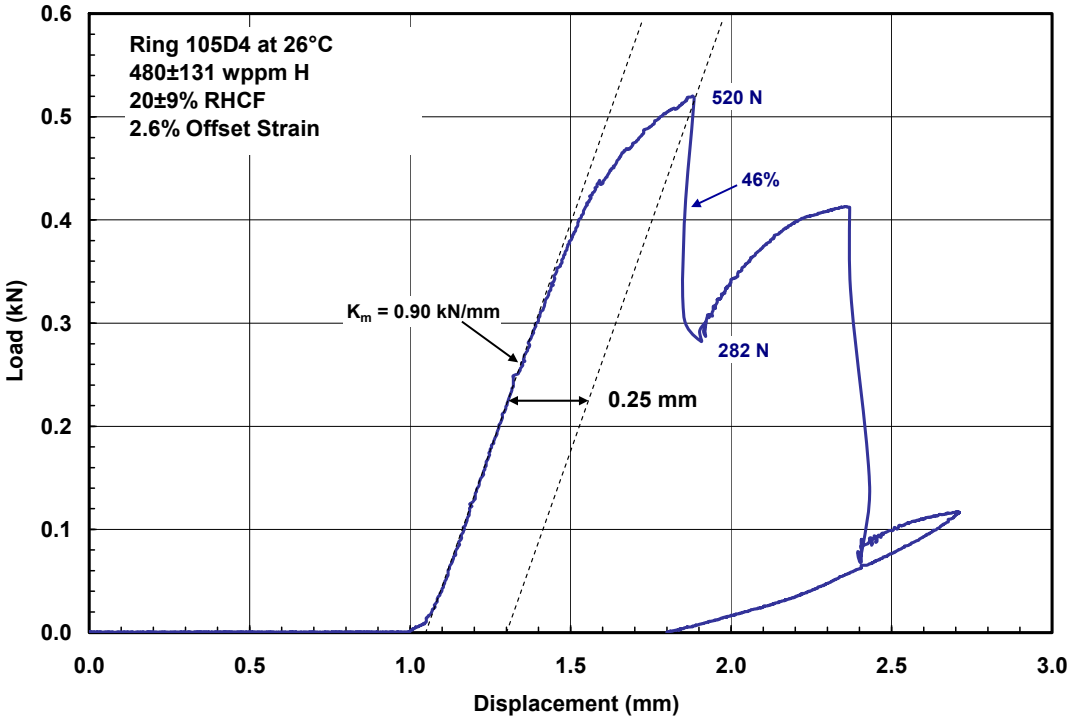

(a) 26°C

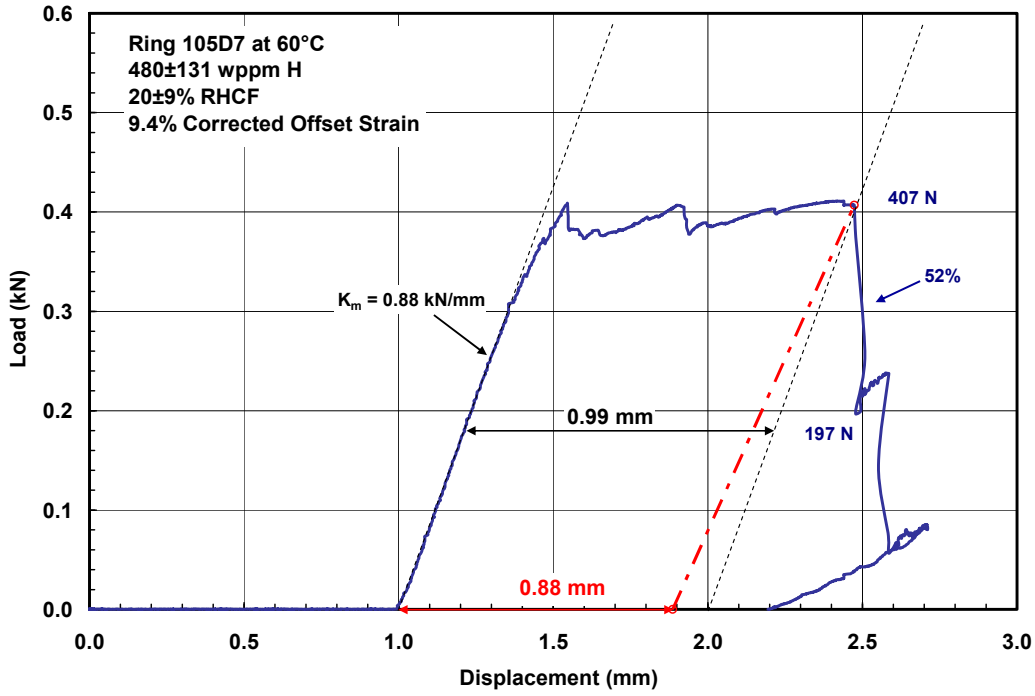

(b) 60°C

Figure 35. Load-displacement curves for tests conducted with samples from the HBU ZIRLO™ rodlet subjected to 3-cycle-cooling RHT at 400°C and peak hoop stress of 90 MPa. RCT temperatures were (a) 26°C and (b) 60°C.

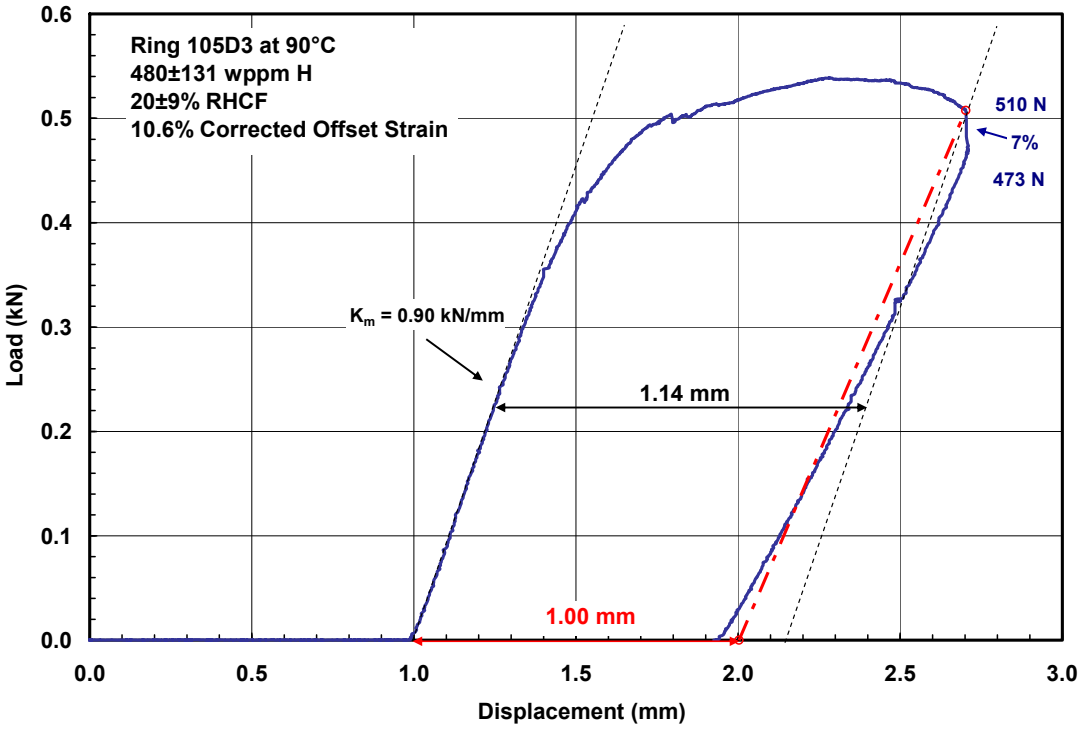

(a) 90°C

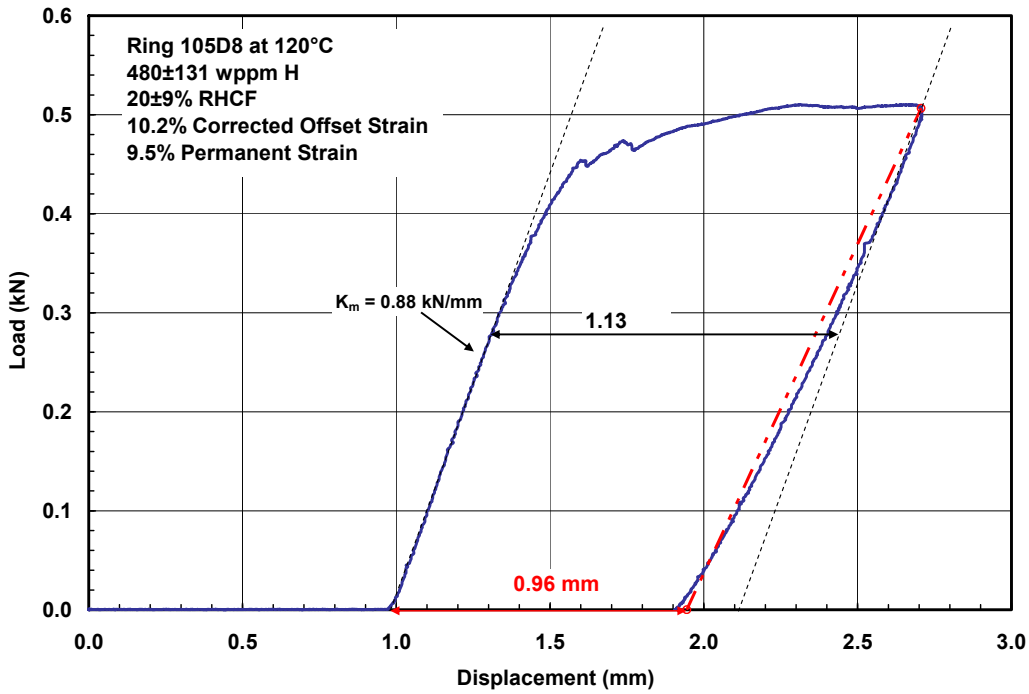

(b) 120°C

Figure 36. Load-displacement curves for tests conducted with samples from the HBU ZIRLO™ rodlet subjected to 3-cycle-cooling RHT at 400°C and peak hoop stress of 90 MPa. RCT temperatures were (a) 90°C and (b) 120°C.

5. DISCUSSION

Ductile-to-Brittle Transition Temperature (DBTT)

Previously, it was established that as-irradiated HBU M5® and ZIRLO™ were highly ductile in response to ring-compression loading at RT (DBTT <20°C). However, it was also demonstrated that following simulated drying and storage at peak conditions of 400°C (NRC-recommended limit) and hoop stresses ≥110 MPa significant radial-hydride precipitation occurred. These radial hydrides caused an increase in DBTT values: ≥70°C for HBU M5® and ≥125°C for HBU ZIRLO™. The opposite trends were observed for HBU Zry-4. HBU Zry-4 exhibited a low sensitivity to radial hydride precipitation and a high sensitivity to total C_H and distribution of circumferential hydrides. As-irradiated HBU Zry-4 with 640 wppm average C_H and >840 wppm local C_H was brittle at ≤90°C (testing limit). After subjecting HBU Zry-4 to the same simulated drying-storage conditions used for HBU M5® and ZIRLO™, the DBTT actually decreased due to the lower C_H of the samples: (a) 55°C DBTT for Zry-4 with 615 wppm average C_H and 720 wppm local C_H following simulated drying-storage at 140-MPa peak hoop stress and (b) <20°C DBTT for Zry-4 with 520 wppm average C_H and 660 wppm local C_H following simulated drying-storage at 110-MPa peak hoop stress at 400°C. It should be noted that HBU ZIRLO™ samples also had high C_H. However, most of the circumferential hydrides were concentrated in hydride rims that were ≤15% of the cladding wall thickness.

In the current work, it was demonstrated that as-irradiated HBU Zry-4 with only 300 wppm C_H was highly ductile. Thus, the embrittlement previously observed was clearly due to the density and radial distribution of circumferential hydrides and not to embrittlement of the Zry-4 metal matrix.

Tests were also conducted with HBU M5® and ZIRLO™ at lower drying-storage stresses in order to determine peak stresses at 400°C that resulted in DBTT values ≤20°C. By lowering the peak drying-storage stress to 90 MPa, the DBTT values for these alloys satisfied the target DBTT value: (a) <20°C for HBU M5® and 20°C for HBU ZIRLO™. After simulated drying-storage at 90-MPa peak hoop stress, the ductility of HBU M5® was so high at 20°C that it is likely the DBTT would be ≤20°C for a peak hoop stress close to 100 MPa. An additional test was conducted with HBU ZIRLO™ after 80-MPa peak drying-storage hoop stress. The DBTT for this material was <20°C.

In parallel with conducting ring-compression tests to determine ductility in response to hoop bending loading, detailed metallographic examinations were performed to gain a basic understanding of the mechanisms responsible for embrittlement. In particular, the effective lengths of radial hydrides across the cladding wall (i.e., the radial-hydride continuity factor, RHCF) were measured. A strong correlation was found between RHCF and peak drying-storage hoop stress. For HBU ZIRLO™, the RHCF decreased from 65% to 30% to 19% (20°C DBTT) to 9% as the peak drying-storage hoop stress decreased, respectively, from 140 MPa to 110 MPa to 90 MPa (20°C DBTT) to 80 MPa. A similar trend was observed for HBU M5® except that higher RHCF values were required to induce embrittlement. This was due to the relatively low C_H (<100 wppm) of the M5® samples. Radial hydrides in M5® tended to be thinner and spaced farther apart than those observed in HBU ZIRLO™ with average C_H in the range of 350 to 650 wppm. For HBU M5®, the RHCF decreased from 72% to 61% to 31% (<20°C DBTT) as the peak simulated drying-storage hoop stress was decreased from 140 MPa to 110 MPa to 90 MPa. Thus, it was demonstrated that HBU M5® with its recrystallized-annealed microstructure has high sensitivity to radial-hydride precipitation compared to stress-relief-annealed ZIRLO™, but it also has lower susceptibility to radial-hydride-induced embrittlement.

Drying Cycles

The reference temperature history for simulated drying-storage tests was based on single-cycle heating-cooling. Samples were heated to 400°C and held at 400°C for one hour prior to cooling at a controlled rate of 5°C/h. Drying, as well as storage, is limited to 400°C cladding temperature (NRC ISG-11, Rev. 3 recommended limit), and the Limiting Conditions of Operation in the Technical Specifications generally calls for holding ≤3-torr moisture for 30 minutes before termination of vacuum drying. ISG-11, Rev. 3 states "During loading operations, repeated thermal cycling (repeated heat-up/cool-down cycles) may occur but should be limited to fewer than 10 cycles, with cladding temperature variations that are less than 65°C (117°F) each cycle." Multiple drying cycles have been associated with increased radial hydride precipitation and DBTT; however, this is based on results for non-irradiated, pre-hydrided Zry-4 cladding subjected to relatively high hoop stress (e.g., 150 MPa) [11]. A test was conducted with HBU ZIRLO™ subjected to three simulated drying cycles. Two heating-cooling cycles (with 100°C ΔT and 5°C/h cooling) were added to the reference temperature history prior to final cooling at 5°C/h. The peak hoop stress was maintained at 90 MPa to obtain a direct comparison between one-cycle and three-cycle cooling. The results showed that the effective length of radial hydrides and the DBTT were unaffected by the additional cooling cycles at the ISG-11 Rev. 3 limit of 90 MPa.

NRC ISG–24

The DBTT data obtained by Argonne earlier for NRC on HBU Zircaly-4 and ZIRLO™ cladding alloys were used in a key reference supporting the recent NRC Interim Staff Guidance (ISG)-24, "The Use of a Demonstration Program as Confirmation of Integrity for Continued Storage of High Burnup Fuel Beyond 20 Years, Revision 0" [12]. ISG-24 provides guidance for the storage of HBU fuels for periods greater than 20 years and specifies that the applicant may use the results of a completed or an ongoing demonstration, in conjunction with an actively updated aging management program (AMP), as an acceptable means for confirming that the canister or cask contents satisfy the applicable regulations. Since limited AMP action can be taken inside a sealed canister, the AMP must ensure that the time-limited aging analysis (TLAA) associated with the aging degradation phenomenon for HBU cladding integrity is updated with new information as it becomes available. ISG-24 further specifies that the TLAA and AMP should be periodically reevaluated and updated whenever new data from the demonstration or other short-term tests or modeling indicate potential degradation of the fuel or deviation from the assumptions of the TLAA or AMP. The updated TLAA and AMP should be submitted to the NRC for review and approval, and will be subject to inspection. Details on the AMPs and TLAAs required for managing aging effects on dry cask storage systems for extended storage and transportation of used fuel have been documented [13], particularly the AMP IV.M5 Canister/Cask Internals Structural and Functional Integrity Monitoring Program and TLAA III.1 Identification of TLAAs that address potential embrittlement due to hydride reorientation in HBU PWR cladding alloys.

It should be noted that ISG-24 specifies the general requirements for a demonstration program for storage of HBU fuel beyond 20 years to support a license or CoC application The data obtained by Argonne for DOE on HBU PWR cladding alloys (Zircaloy 4, ZIRLO™, M5®), as before, will be shared with NRC and industry and contribute directly to help establish the technical basis for extended storage and transportation of HBU fuel.

Recommended Additional Work

Additional testing should be performed to address potential embrittlement of HBU PWR cladding alloys under simulated drying conditions, including the effects of multiple drying cycles, to help determine the processing parameters during drying/transfer operations, such as stress, temperature, cooling rate, temperature cycles, etc., that would minimize formation of radial hydrides and embrittlement of HBU PWR cladding alloys. Lower peak temperatures (e.g., 350°C), realistic end-of life gas pressures and thus cladding hoop stresses [14], with and without temperature cycling, should be investigated to determine

the DBTT values. In addition, axial and hoop tensile properties of as-irradiated HBU PWR cladding alloys should be measured within a relevant temperature range (e.g., 20°C to 100°C) for long-term storage. If axial tensile properties are measured, hoop tensile properties could be determined from the ring-compression data already generated by means of a finite-element model. Mechanical properties data for as-irradiated and post-drying/storage HBU PWR cladding alloys are of immediate value to licensing actions related to transportation and long-term storage of HBU fuel.

This page intentionally blank.

REFERENCES

[1] K.J. Geelhood, W.G. Lusher, and C.E. Beyer, *PNNL Stress/Strain Correlation for Zircaloy*, PNNL-17700, July 2008.

[2] Nuclear Regulatory Commission 2003 Interim Staff Guidance (ISG)-11, Revision 3, "Cladding Considerations for the Transportation and Storage of Spent Fuel," November 2003. [ML033230335 at http://www.nrc.gov/reading-rm/adams.html]

[3] NRC Public Meeting to Obtain Stakeholder Feedback on Enhancements to the Licensing and Inspection Programs for Spent Fuel Storage and Transportation under 10 CFR Parts 71 and 72, August 16–17, 2012, Rockville, MD. [http://www.nrc.gov/public-involve/conference-symposia/2012-sfst-lic-process-conf.html]

[4] M.C. Billone, T.A. Burtseva, and Y. Yan, *Ductile-to-Brittle Transition Temperature for High-Burnup Zircaloy-4 and ZIRLO™ Cladding Alloys Exposed to Simulated Drying-Storage Conditions*, ANL-13/13 (Sept. 2012); NRC ADAMS ML12181A238.

[5] M.C. Billone, T.A. Burtseva, and R.E. Einziger, "Ductile-to-brittle transition temperature for high-burnup cladding alloys exposed to simulated drying-storage conditions," J. Nucl. Mater. 433, 431–448 (2013).

[6] M.C. Billone, T.A. Burtseva, J.P. Dobrzynski, D.P. McGann, K. Byrne, Z. Han, and Y.Y. Liu, *Phase I Ring Compression Testing of High-Burnup Cladding*, FCRD-USED-2012-000039, Dec. 31, 2011.

[7] M.C. Billone, T.A. Burtseva, and Y.Y. Liu, *Baseline Studies for Ring Compression Testing of High-Burnup Fuel Cladding*, FCRD-USED-2013-000040 (ANL 12/58), Nov. 23, 2012.

[8] M.C. Billone, T.A. Burtseva, and Y.Y. Liu, "Effects of Drying and Storage on High-Burnup Cladding Ductility," Proc. IHLRWMC, Albuquerque, NM, April 28−May 2, 2013, Paper 6973, 1106–1113 (2013).

[9] M.C. Billone, T.A. Burtseva, and Y.Y. Liu, "Baseline Properties and DBTT of High-Burnup PWR Cladding Alloys," Proc. PATRAM 2013, San Francisco, CA, August 18–23, 2013 (2013).

[10] M. Aomi, T. Baba, T. Miyashita, K. Kaminura, T. Yasuda, Y. Shinohara, and T. Takeda, "Evaluation of Hydride Reorientation and Mechanical Properties for High-Burnup Fuel-Cladding Tubes in Interim Dry Storage," J of ASTM Intl, JAI101262 (2008). [www.astm.org]

[11] H.C. Chu, S.K. Wu, and R.C. Kuo, "Hydride reorientation in Zircaloy-4 cladding," J. Nucl. Mater. 373 (2008) 319–327.

[12] NRC Interim Staff Guidance (ISG)-24: "The Use of a Demonstration Program as Confirmation of Integrity for Continued Storage of High Burnup Fuel Beyond 20 Years, Revision 0," draft, June 2013.

[13] O. Chopra et al., "Managing Aging Effects on Dry Cask Storage Systems for Extended Long-Term Storage and Transportation of Used Fuel, Rev. 1," FCRD-UFD-2013, 000294 (ANL-13/15), September 30, 2013.

[14] A. J. Machiels, J.Y.R. Rashid, D.J. Sutherland, and W.F. Lyon, "Cladding Hoop Stresses in Spent PWR Fuel – Determination of Rod Internal Pressure as Initial Condition for Dry Storage," *Proc. International Conf. on Packaging and Transport of Radioactive Materials (PATRAM 2013)*, San Francisco, CA, August 18–23, 2013.